SILICOFCM

Project Title: *In Silico* trials for drug tracing the effects of sarcomeric protein mutations leading to familial cardiomyopathy

Project acronym: SILICOFCM

Grant Agreement number: 777204

Coordinating Institution:
Bioengineering Research and Development Center BioIRC doo Kragujevac, BIOIRC

Start date: 1st June 2018

Duration: 45 months

WP number, Deliverable number and Title	**WP8 Report to FDA or EMA** **D8.2 Computational pipelines for drug testing**
Related Task	**Task 8.2 Set up R&D computation pipelines for drug testing**
Lead Beneficiary	IIT
Deliverable Type	Other
Distribution Level	Public
Document version	v.2.0
Contractual Date of Delivery	31/05/2021
Actual Date of Delivery	07/06/2021
Date of delivery of the revised version	02/11/2021

Authors	IIT (Srboljub Mijailovich), BIOIRC (Nenad Filipovic, Milos Kojic, Boban Stojanovic, Milos Ivanovic, Momcilo Prodanovic, Danica Prodanovic, Bogdan Milicevic, Miljan Milosevic, Vladimir Simic, Vladimir Geroski, Smiljana Djorovic, Aleksandra Vulovic)
Contributors	UOI, SBG, R-Tech
Reviewers	UOI (Nikolaos Tachos, Mary Roumpy), SBG (Michele Mattioni), ICVDV (Lazar Velicki)

This project has received funding from the European Union's Horizon 2020 research and innovation programme under grant agreement No 777204

Version history

Version	Description	Date of completion
0.1	Created ToC	05/04/2021
0.2	Included examples for drug testing with different affects (Section 3)	21/04/2021
0.3	Completed Section 2	11/05/2021
0.4	Incorporated MUSICO and PAK Solver tool in Section 4	21/05/2021
0.5	Incorporated Section 4.3 and refined Section 4	27/05/2021
0.6	Completed Section 3	01/06/2021
0.7	Completed Section 1, Section 5 and Section 6 and sent for the review	03/06/2021
0.8	Revision of document (SBG, UOI)	04/06/2021
0.9	Final refinements of the document	05/06/2021
1.0	Final version submitted to EC	07/06/2021
1.1	The Section *Computational Cloud Platform* - transferred in the D8.1	10/10/2021
1.2	Updated Section 2	12/10/2021
1.3	Updated Section 3	15/10/2021
1.4	Updated Sections 4 and 5	18/10/2021
1.5	Internal review	20/10/2021
1.6	Proofreading, formatting, abbreviations	29/10/2021
2.0	Final revised version re-submitted to EC	02/11/2021

Disclaimer

*Deliverable Type: Report, Other, ORDP: Open Research Data Pilot, Ethics

**Dissemination Level: PU=Public, CO=Confidential, only for members of the consortium (including Commission Services)

Executive summary

The revised deliverable D8.2 “Computational pipelines for drug testing” corresponds to the work performed within Task 8.2 “2 Set up R&D computation pipelines for drug testing” (M24-M36) of the SILICOFCM project. One of the main purposes of the SILICOFCM platform is to simulate the effects of various drugs on cardiac function; particularly on various cardiomyopathy diseases.

In Section 2, we continue with the description of different drugs which reacted through three characteristic pathways of drug flow: at the level of contractile proteins, at the level of regulation of transient intracellular calcium concentration and at the level tissue remodelling and/or by modulation of blood vessel elasticity, i.e. resistance to blood flow and cardiac output. These drugs are Digoxin, Mavacamten, 2-deoxy adenosine triphosphate (dATP) with fitted parameters from MUSICO. Also, Disopyramide and Mavacamten are described with their effects in the macroscopic parameters inside the SILICOFCM platform.

The results obtained from the PAK solver in the left ventricle model with 20% shorter base length have been presented in Section 3, including the corresponding PV diagrams for different Ca2+ concentrations, displacement (deformation), velocity and pressure field with analysis of ejection fraction and wall elasticity. In addition, different PV diagrams are shown for the inlet and outlet velocity boundary conditions which simulate drug effects on the macroscopic level. Similar results for the left ventricle model with 50% longer base length and 50% thicker lateral wall have been reported. Realistic geometry of the heart model with left chamber and atrium parts surrounded by solid wall and standard inlet and outlet velocity profiles have also been presented in Section 3.

The whole heart activation simulation from lead II ECG signal at various time points on the ECG signal have been analysed for several patients from SILICOFCM clinical partners. The activation sequences correspond to the ECG signal. The simulated ECG on the surface body with real ECG measurement at V1 have been compared in Section 3.

Finally, conclusions have been reported in Section 5.

The performed work is related to WP4, WP5 and WP6, and should be read together with D8.1 “Workflow for drug testing”. In addition, the document is interlinked with D8.3 “Interface drug database”. The work that is being performed within the Task 8.2, as well as within the whole WP8, is a continuous process, and will be concluded in D8.4 “Development report tool”.

Table of Contents

List of Figures

List of Tables

List of Abbreviations

Abbreviation	Explanation	Abbreviation	Explanation
ADP	Adenosine Diphosphate	**LV**	Left Ventricle
ATP	Adenosine Triphosphate	**LVEF**	Left Ventricle Ejection Fraction
ARNI	Angiotensin Receptor Neprilysin Inhibitor	**LVEDV**	Left Ventricular End-Diastolic Volume
AWS	Amazon Web Services	**LVESV**	Left Ventricular End-Systolic Volume
CWL	Common Workflow Language	**LVH**	Left Ventricular Hypertrophy
dATP	2-deoxy adenosine triphosphate	**LVIDd**	Left Ventricular End-Diastolic Diameter
DBP	Diastolic Blood Pressure	**LVID**	Left Ventricular End-Systolic Diameter
DCM	Dilated Cardiomyopathy	**LVMI**	Left Ventricular Mass Index
ECG	Electrocardiogram	**LVP**	Left Ventricle Pressure
EF	Ejection Fraction	**MP**	Mijailovich - Prodanovic
FAIR	Findable, Accessible, Interoperable and Reusable	**MUSICO**	MUscle SImulation COde
FCM	Familial Cardiomyopathy	**PV**	Pressure - Volume
FDA	Food and Drug Administration	**PW**	Posterior Wall
FE	Finite Element	**PWTd**	End-Diastolic Posterior Wall Thickness
FS	Fractional Shortening of LV	**SBG**	Seven Bridges Genomics
HCM	Hypertrophic Cardiomyopathy	**SBP**	Systolic Blood Pressure
HFrEF	Heart Failure and Reduced Ejection Fraction	**STL**	Stereolithography
IVS	Interventricular Septum	**TR**	Tricuspid Regurgitation
IVSd	End-Diastolic Septal Wall Thickness	**WT**	Wild Type

1. Introduction

In silico clinical trials allow testing of drugs in "virtual patients" using computational modelling and a variety of simulation techniques. This approach can detect possible drug issues in the beginning of drug development, before they are tested on humans. In silico computational models are used to evaluate various treatments on specific diseases, but also to test a larger set of different conditions such as dosing. These models are used to model human diseases, which can be limited by in-vitro/vivo techniques. *In silico* modelling offers more practical and economical experiments compared to clinical studies and animal experiments. Additionally, *in silico* trials have not been limited by COVID-19 restriction as the majority of conventional trials have been during the COVID-19 pandemic.

SILICOFCM aims to develop a computational platform for *in silico* clinical trials of Familial cardiomyopathies (FCMs) that would take into consideration a comprehensive list of patient-specific features (genetic, biological, pharmacologic, clinical, imaging and patient-specific cellular aspects) capable of optimizing and testing medical treatment strategy with the purpose of maximizing positive therapeutic outcome, avoiding adverse effects and drug interactions, preventing sudden cardiac death, shortening time between the drug treatment commencement and the desired result.

SILICOFCM is a multi-modular, innovative *in silico* clinical trials solution for the design and functional optimization of the whole heart performance and monitoring effectiveness of pharmacological treatment, with the aim to reduce animal studies and human clinical trials. The SILICOFCM platform is based on the integrated multidisciplinary and multiscale methods for the analysis of patient-specific data and development of patient-specific models for monitoring and assessment of patient condition from initial through the progression of disease.

One of the aims of the SILICOFCM is to become a respectable *in silico* solution with developed computational cloud platform in all areas and levels of health care by combining the data from multiple data sets collected at multiple scales with sophisticated and continuously developing computational models and, therefore, following the information flow across all length scales from a gene mutation to organ dysfunction. Thus, the integrated SILICOFCM cloud platform for the simulation of various drugs on cardiac function, particularly on the various cardiomyopathy diseases has been described. Different drugs such as Digoxin, Mavacamten, 2-deoxy adenosine triphosphate (dATP) with fitted parameters from MUSICO which reacted through three characteristic pathways of drug flow are included in the SILICOFCM drug testing. Disopyramide and Mavacamten are described with their effects in the macroscopic parameters inside the SILICOFCM platform.

In addition, the corresponding PV diagrams in the PAK finite element solver for different Ca2+ concentrations, displacement (deformation), velocity and pressure field with analysis of ejection fraction and wall elasticity have been presented. The activation sequences which correspond to ECG signals were compared with real ECG measurement at V1 from clinical partners.

A number of different scenarios of using SILICOFCM platform for various drugs testing for basic cardiac function have been presented with an initial comparison of the in silico with the main clinical parameters such as PV diagram, systemic pressure, input and output blood flow velocity from left ventricle, ejection fraction, ECG measurements on body surface on the real patients. This approach is very promising for the future use of the SILICOFCM platform as software as a medical device, as well as for research purposes.

The presented deliverable is interlinked and should be read together with deliverable D8.1 "Workflow for drug testing".

1.1 Relation to the DoA

The following Table presents the DoA description of Task 8.2 and how this deliverable addresses the description of the Task.

DoA Task Description	Addressed by D8.2
Integration of the computational tools from WP4, WP5 and WP6 in order to simulate all drug testing during development. Computational platform will be implemented on cloud platform. This computational platform will include the following components: (i) Client application Layer available through the web (access layer using a web browser), (ii) Cloud server computational Layer (data processing layer and compute engines including Restful services' providers), (iii) Data and Models management Layer, (iv) Cloud data repository Layer.	The presented document addresses the DoA description in the following: The SILICOFCM cloud platform has been integrated, and its architecture is briefly presented in Section 3.1 in D8.1, as well as the workflow management (Section 3.2 in D8.1). The SILICOFCM architecture consists of five layers: i) Hardware, ii) Security, iii) Workflow, iv) Back-end, and v) Front-end. The workflow management is organised following FAIR data principles. In addition, the SILICOFCM running drug testing workflows on AWS are described in Section 3.3 in D8.1. The D8.2 also includes the use cases of drug testing, included in Section 2. Several different drugs have been tested, affecting changes in kinetic and macroscopic parameters. Also, the PAK and ECG modules for drug testing are presented (Section 3), giving the main updates and latest achievements in drug testing.

1.2 Reviewer's recommendations and how we addressed them

After the project review meeting that was held on July 5th 2021, the consortium received the report which stated that the deliverable was rejected and sent back for updates. The reviewers' comments and suggestions are shown in the following table, as well as the consortium's responses.

Reviewer's recommendations	How we addressed them?
A major issue of this document is that the differentiation between the "computational pipelines" it needs to address, and the workflows covered in D8.1, is not sufficiently clear. The document fails to explain the delta between the two deliverables and this remains a shortcoming throughout the document.	The differentiation between the "computational pipelines" and the workflows covered in D8.1 is clearer now. We moved Chapter 3 which describes SILICOFCM architecture cloud platform from D8.2 to D8.1.
For example, Chapter 3 complements the content of Chapter 3 in D8.1. They both deal with drug testing studies based on SILICOFCM facilities, but it is not sufficiently detailed why these studies are split in the two deliverables. The same is valid also for Chapter 4, where additional studies based on the PAK Solver are presented. For example, a much clearer split of content would be to have D8.1	The Chapters 3 and 4 in D8.1 (now Chapters 4 and 5) as well as Chapters 3 and 4 in D8.2 (now Chapters 2 and 3) are revised in order to split content where in D8.1 we discuss designs of the workflows and in D8.2 implementation and testing.

dealing with the design of the workflows and D8.2 with the implementation and testing.	
The analysis of left ventricular pressure-volume loops available in D8.2 and D8.1 is questionable in that they mostly take into account the effects induced by the administration of drugs on the left ventricle.	We have fixed a bug in the software and now pressure-volume loops in D8.2 look more reasonable.
The results presented in D8.1 and D8.2 (left ventricular P-V loops) have to be revisited as they do not represent real clinical data. These two deliverables should be reviewed and resubmitted before the end of October 2021, with a focus on highlighting the assumptions made, current limitations and alternative approaches.	We updated P-V loops and highlighted all the assumptions made, current limitation and alternative approaches.

2. SILICOFCM Workflow for drug testing – Case studies

A global architecture of the SILICOFCM drug testing workflow is shown in Figure 3 in D8.1. However, the drug actions are different for threating variety of symptoms associated with cardiomyopathies. Thus, we provided three pathways through a general workflow for different scenarios shown in Figure 1. In particular, simulated drugs with MUSICO are separated in three major groups defined by the principal action of specific drugs, as for example, on modulating calcium transients or changing kinetics of contractile proteins. Each group consists of two subgroups based on the type of cardiomyopathy:

1. Modulation of [Ca^{2+}] transients (Figure 1A)
    a. HCM – Disopyramide, which lowers peak and baseline levels of [Ca^{2+}] transient during twitch contractions[1],
    b. DCM – Digoxin, which increases peak of [Ca^{2+}] transient during twitch contractions, but does not change time to peak and relaxation time[2],
2. Changes in kinetic parameters (Figure 1B)
    a. HCM – Mavacamten, which is associated with regulation of kinetics rates of transition between disordered myosin detached states and ordered parked state[3],
    b. DCM – dATP, which modulates crossbridge cycle rates[4,5],
3. Changes in macroscopic parameters (Figure 1C)
    a. HCM – Entresto®, which acts on remodelling of heart ventricle walls and modulates the elasticity of blood vessels, typically reducing resistance to blood flow and improving cardiac output in HCM.

Since drugs in groups 1 and 2 directly affect MUSICO and MP surrogate parameters, we were able to predict with our tools the outcome on force generation in sarcomeres during twitch contractions.

2.1 Drugs that modulate [Ca^{2+}] transients

The workflow for testing these types of drugs is shown in Figure 1A. The experimental observations in action potentials and changes in ionic currents are simulated using O'Hara-Rudy electro-physiological model[6] that produces intracellular calcium transient as an input for MUSICO and MP surrogate models.

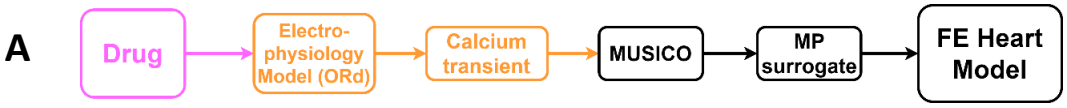

[1] Coppini, R., Ferrantini, C., Pioner, J. M., Santini, L., Wang, Z. J., Palandri, C., ... & Sherrid, M. V. (2019). Electrophysiological and contractile effects of disopyramide in patients with obstructive hypertrophic cardiomyopathy: a translational study. JACC: Basic to Translational Science, 4(7), 795-813.

[2] Morgan, J. P., Chesebro, J. H., Pluth, J. R., Puga, F. J., & Schaff, H. V. (1984). Intracellular calcium transients in human working myocardium as detected with aequorin. Journal of the American College of Cardiology, 3(2), 410-418.

[3] Ma, W., Marcus, M., Anderson, R. L., Gong, H., Wong, F. L., del Rio, C. L., Irving, T. The super-relaxed state and length dependent activation in porcine myocardium. (in press).

[4] Regnier, M., Lee, D. M., & Homsher, E. (1998). ATP analogs and muscle contraction: mechanics and kinetics of nucleoside triphosphate binding and hydrolysis. Biophysical journal, 74(6), 3044-3058.

[5] Regnier, M., Rivera, A. J., Chen, Y., & Chase, P. B. (2000). 2-deoxy-ATP enhances contractility of rat cardiac muscle. Circulation research, 86(12), 1211-1217.

[6] O'Hara, T., Virág, L., Varró, A., & Rudy, Y. (2011). Simulation of the undiseased human cardiac ventricular action potential: model formulation and experimental validation. PLoS Comput Biol, 7(5), e1002061.

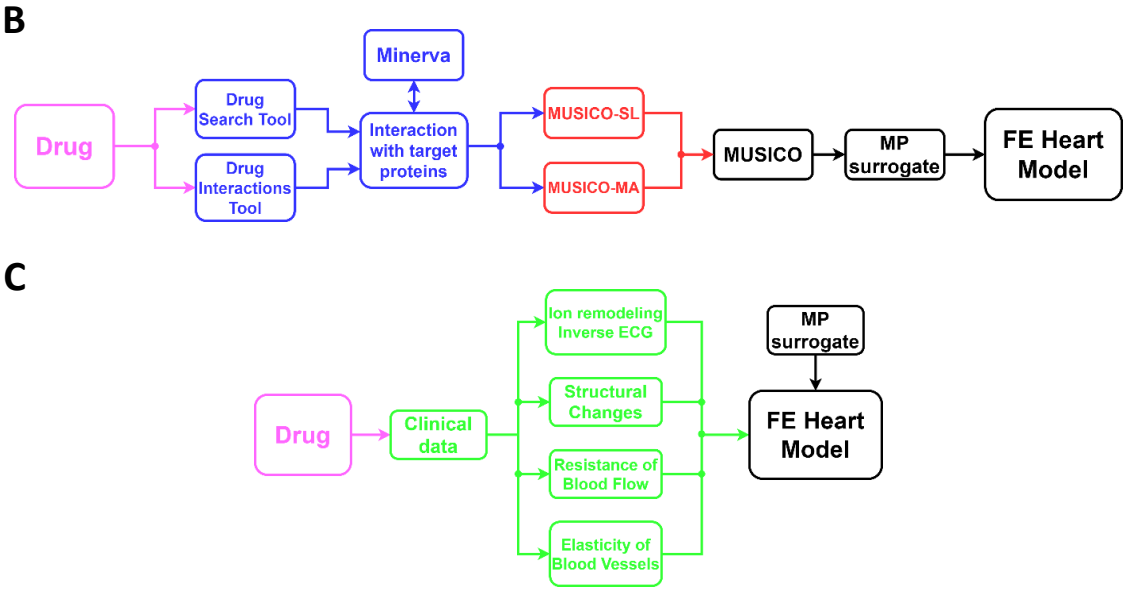

Figure 1. Three pathways of drug action in SILICOFCM drug testing workflow. A) By modulation of calcium transient through changes in ionic currents or membrane properties, B) through changes in kinetic of contractile proteins, C) through macroscopic structural and boundary condition changes.

2.1.1 Disopyramide

Disopyramide, classified as a type I antiarrhythmic (i.e., a sodium channel blocker) is a potent negative inotrope[7]. It has been used to decrease left ventricular outflow tract obstruction in obstructive HCM since first reports in the early 1980's[8,9]. Until recently, it was not known whether the drug had direct effects on Excitation-Contraction Coupling or on the actin-myosin interaction. Recent work by Coppini et al[1] on human HCM cardiomyocytes and trabeculae has shown that disopyramide inhibits multiple ion channels, leading to lower Ca2+ transients and twitch force with no direct inhibitory effects on myofilament function. In addition, disopyramide does not exert proarrhythmic effects in vitro; rather it shortens action potentials showing potential for reduced arrhythmic propensity. The observation that disopyramide is a negative inotrope that does not interfere with sarcomere protein function makes this drug likely compatible with the new class of allosteric myosin modulators (e.g., Mavacamten) currently under successful clinical investigation for use in HCM[10].

The key HCM features include significant increase in thickness of heart walls, increased cardiac muscle contractility and, in some cases increase, fibrosis. Disopyramide decreases intracellular calcium transient, by both decreasing the twitch [Ca2+] peak and the level of basal calcium concentration

[7] Pollick, C., Giacomini, K. M., Blaschke, T. F., Nelson, W. L., Turner-Tamiyasu, K., Briskin, V., & Popp, R. L. (1982). The cardiac effects of d-and l-disopyramide in normal subjects: a noninvasive study. Circulation, 66(2), 447-453.

[8] Pollick, C. (1982). Muscular subaortic stenosis: hemodynamic and clinical improvement after disopyramide. New England Journal of Medicine, 307(16), 997-999.

[9] Sherrid, M. V., Barac, I., McKenna, W. J., Elliott, P. M., Dickie, S., Chojnowska, L., ... & Maron, B. J. (2005). Multicenter study of the efficacy and safety of disopyramide in obstructive hypertrophic cardiomyopathy. Journal of the American College of Cardiology, 45(8), 1251-1258..

[10] Olivotto I, Oreziak A, Barriales-Villa R, Abraham TP, Masri A, Garcia-Pavia P, Saberi S, Lakdawala NK, Wheeler MT, Owens A, Kubanek M, Wojakowski W, Jensen MK, Gimeno-Blanes J, Afshar K, Myers J, Hegde SM, Solomon SD, Sehnert AJ, Zhang D, Li W, Bhattacharya M, Edelberg JM, Waldman CB, Lester SJ, Wang A, Ho CY, Jacoby D (2020). Mavacamten for treatment of symptomatic obstructive hypertrophic cardiomyopathy (EXPLORER-HCM): a randomised, double-blind, placebo-controlled, phase 3 trial. The Lancet, 396(10253), 759-769.

(Figure 2). MUSICO simulations predicted decrease on the peak tension by ~55% and decrease in resting tension by ~50% in the presence of 5 µmol/l of disopyramide, matching the observations of Coppini et al[1]. The parameters used in MUSICO simulations originate from WT human with 100% myosins used in Prodanovic et al.[11] while calcium kinetics is taken from mouse HCM[12] and they are shown in Table 1. For use in FE analysis, the MUSICO simulations are approximately replicated by surrogate model and the surrogate fitted parameters are shown in Table 2.

These simulations can be extended to the whole heart simulations using PAK and Alya solvers to quantitatively assess the effect of drug on cardiac output including decrease in both systolic and diastolic pressures, and the ejection fraction.

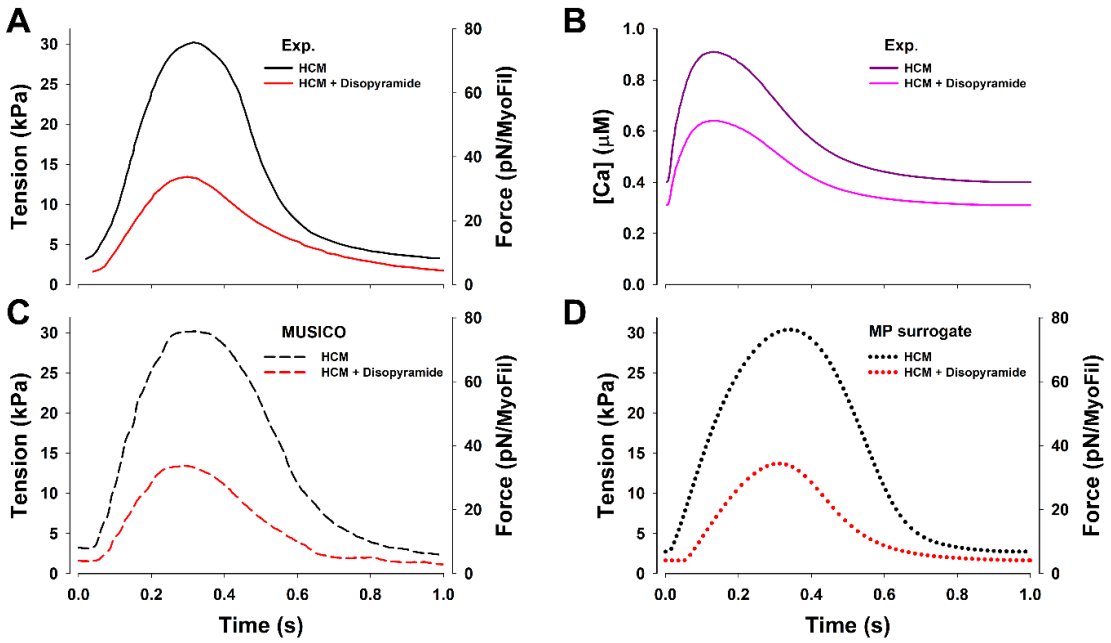

Figure 2. Disopyramide effects on twitch contraction. A) Experimental twitch traces and B) calcium transients. C) MUSICO (*dashed lines*) and D) MP surrogate model (dotted lines) predictions of twitches for HCM sarcomere in presence (red) and without disopyramide (black).

Table 1. MUSICO parameters for HCM in human 100% β myosin sarcomeres

	Description	Parameter	Value
Crossbridge Cycle	Myosin-actin binding rate	k_{+A}	90 s^{-1}
	Myosin-actin detachment rate	k_{-A}	60 s^{-1}
	Myosin stroke cap rate	k_{+Pi_cap}	1000 s^{-1}
	Myosin reverse stroke cap rate	k_{-Pi_cap}	15 s^{-1}
	Power stroke energy	G_{stroke}	-11.3 k_BT
	Working stroke	d	10.5 nm
	Second working stroke	δ	1 nm
	ADP release rate	k_{+D}	60 s^{-1}

[11] Prodanovic M, Geeves MA, Poggesi C, Regnier M, Mijailovich SM: Effect of Myosin Isoform on the Mechanics on Intact Cardiac Trabeculae from Mice, Rats and Humans, J.Gen. Physiol. (in print).

[12] Mijailovich, S. M., Prodanovic, M., Poggesi, C., Powers, J. D., Davis, J., Geeves, M. A., & Regnier, M. (2021). The effect of variable troponin C mutation thin filament incorporation on cardiac muscle twitch contractions. Journal of Molecular and Cellular Cardiology, 155, 112-124.

	ATP binding and myosin detach.	k_{+T}	10^6 s^{-1}	
	Hydrolysis forward rate	k_{+H}	70 s^{-1}	
	Hydrolysis backward rate	k_{-H}	7 s^{-1}	
	Crossbridge stiffness	κ	1.3 pN/nm	
	k_BT at 30°C	k_BT	4.116 pN·nm	
Calcium Kinetics	Calcium binding to TnC equilibrium rate constant	K_{Ca}	WT	10^6 M^{-1}
			HCM	$3.21 \cdot 10^6$ M^{-1}
	Calcium binding to TnC	$\tilde{k}_{Ca}$	$7.54 \cdot 10^7$ M^{-1}·s^{-1}	
	Calcium Dissociation Rate from TnC	k_{-Ca}	WT	75.4 s^{-1}
			HCM	23.52 s^{-1}
	TnI-actin equilibrium rate const. at high Ca^{2+}	λ	WT	10
			HCM	20
	TnI-actin-Ca cooperativity coefficient	ε_o	0.01	
CFC	Tropomyosin pinning angle	ϕ_-	-25°	
	Myosin Tm angular displ.	ϕ_+	10°	
	Angular SD of free CFC	σ_0	29.7°	
	Persistence length of Tm-Tn confined chain	$1/\xi$	50 nm	
Parked State	Transition rate to “parked state”	k_{-PS}	200 s^{-1}	
	Baseline rate	k_{PS}^0	5 s^{-1}	
	Amplitude	k_{PS}^{max}	400 s^{-1}	
	Hill function slope	b	5	
	Half activation point of the Hill function	$[Ca_{50}]$	1 µM	
Sarcomere	Length of Sarcomere	SL	2.2 µM	
	Length of Actin fiber	L_a	1.1 µM	
	Thin filament elastic modulus	AE_a	65 nN	
	Thick filament elastic modulus	AE_m	132 nN	

Table 2. Parameter Values for MP surrogate model for the prediction of the effect of disopyramide on HCM

Parameter	HCM	Disopyramide
SL_0	1.6	1.6
SL_isom	2.2	2.2

LA	1.1	1.1
LM	1.6	1.6
B	0.176	0.176
R_T_0	1.62E+05	$1.62 \cdot 10^5$
x0	0.007	0.007
Ca_50	0.915	0.915
k_on_0	0	0
k_on_Ca	553.70	553.70
k_off_0	100	100
k_off_Ca	150	150
k_lambda_on_0	4200	4200
k_lambda_off_0	375	375
f_0_p	512.22	64.11
h_0	357.72	1019.88
h_0_p	2134.23	1944.29
g_0	173.80	172.32
k_PS_0	0.369	0.292
k_PS_max	3593.58	3335.84
b_param	5	5
Ca_50_PS	1.03	1.061
u	2.357	0.715
w	4.232	4.492
v	3.455	0.253
beta	0	0
eta	0.380	0.125
sigma_p	7.2	7.2
sigma_n	1	1
Stiff_Eq_P1	197.54	197.54
Stiff_Eq_P2	3434.96	3434.96
Stiff_Eq_P3	0	0

2.1.2 Digoxin

Cardioactive glycosides (e.g., Digoxin) have been important in treating congestive heart failure for more than 200 years, in large part because of a positive inotropic effect. The traditional view is that direct Na^+–K^+-ATPase inhibition leads to elevation of $[Na^+]_i$ with consequent gain of cellular and

sarcoplasmic reticulum (SR) [Ca^{2+}] as a result of shifts mediated via the Na^{+}–Ca^{2+} exchanger[13]. That is, with higher $[Na^{+}]_i$, Ca^{2+} extrusion via NCX is reduced and Ca^{2+} influx via NCX may be enhanced. Thus, there can be higher diastolic $[Ca^{2+}]_i$ (closer to threshold for contractile activation), higher SR Ca^{2+} content (causing greater SR Ca^{2+} release during contraction) and even greater Ca^{2+} influx via NCX during the action potential. All of these mechanisms lead to increased Ca^{2+} transient amplitude and peak twitch force. Studies with aequorin injected preparations of human cardiac muscle showed that cardiac glycosides increase twitch force by increasing the amplitude of the Ca^{2+} transient without affecting the time course of the Ca^{2+} transient and that the increase in tension is fully accounted for the increase in systolic free calcium[14].

The Dilated Cardiomyopathy (DCM) results in expansion of the chambers while the muscular wall progressively becomes thinner. In addition, cardiac function in DCM is compromised with decreased cardiac muscle contractility that, in concert with the structural changes of an enlarged left ventricle, reduces systolic function, with an ejection fraction <50%. Digoxin increases intracellular calcium concentration transient (opposite of Disopyramide), by increasing the [Ca^{2+}] peak during twitch contractions but keeping time to peak and relaxation time constant[14,15] (Figure 3).

The increase in intracellular calcium concentration increases heart wall tension, and therefore increases systolic pressure and ejection fraction. The MUSICO simulations predicted dose dependent increase on the peak tension up to twofold. The dose dependence of the [Ca^{2+}] peak during twitch contractions and the peak tensions are shown in Figure 3B. The majority of parameters used in MUSICO simulations originate from WT human with 100% β myosins used in the study of Prodanovic et al.[16] while calcium kinetics is taken from mouse DCM[17] and they are shown in Table 3. The MUSICO simulations are approximated by surrogate model and the surrogate fitted parameters are shown in Table 4, for use in FEA analysis.

The FE simulations of heart using PAK and Alya solvers enable quantitative assessment of the effect of Digoxin on cardiac output including increase in both systolic and diastolic pressures, and the ejection fraction.

[13] Bers, D. (2001). Excitation-contraction coupling and cardiac contractile force (Vol. 237). Springer Science & Business Media.
[14] Morgan, J. P. (1985). The effects of digitalis on intracellular calcium transients in mammalian working myocardium as detected with aequorin. Journal of molecular and cellular cardiology, 17(11), 1065-1075.
[15] Morgan, J. P., Chesebro, J. H., Pluth, J. R., Puga, F. J., & Schaff, H. V. (1984). Intracellular calcium transients in human working myocardium as detected with aequorin. Journal of the American College of Cardiology, 3(2), 410-418
[16] Prodanovic M, Geeves MA, Poggesi C, Regnier M, Mijailovich SM: Effect of Myosin Isoform on the Mechanics on Intact Cardiac Trabeculae from Mice, Rats and Humans, J.Gen. Physiol. (in print).
[17] Mijailovich, S. M., Prodanovic, M., Poggesi, C., Powers, J. D., Davis, J., Geeves, M. A., & Regnier, M. (2021). The effect of variable troponin C mutation thin filament incorporation on cardiac muscle twitch contractions. Journal of Molecular and Cellular Cardiology, 155, 112-124.

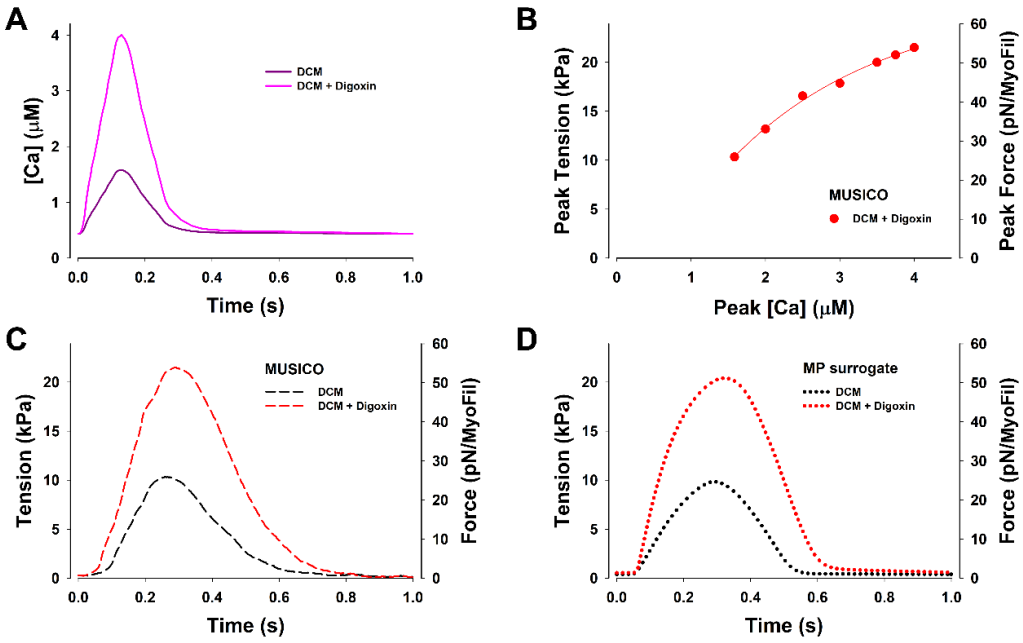

Figure 3. Digoxin effects on twitch contraction. A) Calcium transient predictions for DCM in presence (pink) and without digoxin (purple). B) Peak tension dependence on peak calcium concentration during twitch contractions in presence of increased doses of digoxin. C) MUSICO (*dashed lines*) and D) MP surrogate model (dotted lines) predictions of twitches for DCM sarcomere in presence (red) and without digoxin (black).

Table 3. MUSICO parameters for HCM in human 100% β myosin sarcomeres

	Description	Parameter	Value	
Crossbridge Cycle	Myosin-actin binding rate	k_{+A}	90 s^{-1}	
	Myosin-actin detachment rate	k_{-A}	60 s^{-1}	
	Myosin stroke cap rate	k_{+Pi_cap}	1000 s^{-1}	
	Myosin reverse stroke cap rate	k_{-Pi_cap}	15 s^{-1}	
	Power stroke energy	G_{stroke}	-11.3 k_BT	
	Working stroke	d	10.5 nm	
	Second working stroke	δ	1 nm	
	ADP release rate	k_{+D}	60 s^{-1}	
	ATP binding and myosin detach.	k_{+T}	10^6 s^{-1}	
	Hydrolysis forward rate	k_{+H}	70 s^{-1}	
	Hydrolysis backward rate	k_{-H}	7 s^{-1}	
	Crossbridge stiffness	κ	1.3 pN/nm	
	k_BT at 30 °C	k_BT	4.116 pN·nm	
Calcium Kinetics	Calcium binding to TnC equilibrium rate constant	K_{Ca}	WT	10^6 M^{-1}
			HCM	$3.21 \cdot 10^6$ M^{-1}
	Calcium binding to TnC	$\tilde{k}_{Ca}$	$7.54 \cdot 10^7$ $M^{-1} \cdot s^{-1}$	

	Calcium Dissociation Rate from TnC	k_{-Ca}	WT	75.4 s^{-1}
			HCM	23.52 s^{-1}
	TnI-actin equilibrium rate const. at high Ca^{2+}	λ	WT	10
			HCM	20
	TnI-actin-Ca cooperativity coefficient	ε_o	0.01	
CFC	Tropomyosin pinning angle	ϕ_-	-25°	
	Myosin Tm angular displ.	ϕ_+	10°	
	Angular SD of free CFC	σ_0	29.7°	
	Persistence length of Tm-Tn confined chain	$1/\xi$	50 nm	
Parked State	Transition rate to "parked state"	k_{-PS}	200 s^{-1}	
	Baseline rate	k_{PS}^0	5 s^{-1}	
	Amplitude	k_{PS}^{max}	400 s^{-1}	
	Hill function slope	b	5	
	Half activation point of the Hill function	$[Ca_{50}]$	1 µM	
Sarcomere	Length of Sarcomere	SL	2.2 µM	
	Length of Actin fiber	L_a	1.1 µM	
	Thin filament elastic modulus	AE_a	65 nN	
	Thick filament elastic modulus	AE_m	132 nN	

Table 4. Parameter Values for MP surrogate model for the prediction of the effect of disopyramide on HCM

Parameter	HCM	Disopyramide
SL_0	1.6	1.6
SL_isom	2.2	2.2
LA	1.1	1.1
LM	1.6	1.6
B	0.176	0.176
R_T_0	1.62E+05	$1.62 \cdot 10^5$
x0	0.007	0.007
Ca_50	0.915	0.915
k_on_0	0	0
k_on_Ca	553.70	553.70
k_off_0	100	100
k_off_Ca	150	150

k_lambda_on_0	4200	4200
k_lambda_off_0	375	375
f_0_p	512.22	64.11
h_0	357.72	1019.88
h_0_p	2134.23	1944.29
g_0	173.80	172.32
k_PS_0	0.369	0.292
k_PS_max	3593.58	3335.84
b_param	5	5
Ca_50_PS	1.03	1.061
u	2.357	0.715
w	4.232	4.492
v	3.455	0.253
beta	0	0
eta	0.380	0.125
sigma_p	7.2	7.2
sigma_n	1	1
Stiff_Eq_P1	197.54	197.54
Stiff_Eq_P2	3434.96	3434.96
Stiff_Eq_P3	0	0

2.2 Drugs that affect changes in kinetic parameters

The workflow for testing these types of drugs is shown in Figure 1B. The experimental observations in the experiments in vitro that quantify the effect of specific drug (dose) are used for the estimation of parameters for MUSICO and MP surrogate models.

2.2.1 Mavacamten

Mavacamten (MYK-461) is a promising small molecule designed to act as an allosteric inhibitor of sarcomeric myosins[18] and has already been successfully used in clinical trials for treatment of HCM[19].

[18] Green, E. M., Wakimoto, H., Anderson, R. L., Evanchik, M. J., Gorham, J. M., Harrison, B. C., Henze, R. Kawas, J.D. Oslob, H.M. Rodriguez, Y. Song, W. Wan, L.A. Leinwand, J.A. Spudich, R.S. McDowell, J.G. Seidman & Seidman, C. E. (2016). A small-molecule inhibitor of sarcomere contractility suppresses hypertrophic cardiomyopathy in mice. Science, 351(6273), 617-621.
[19] Olivotto I, Oreziak A, Barriales-Villa R, Abraham TP, Masri A, Garcia-Pavia P, Saberi S, Lakdawala NK, Wheeler MT, Owens A, Kubanek M, Wojakowski W, Jensen MK, Gimeno-Blanes J, Afshar K, Myers J, Hegde SM, Solomon SD, Sehnert AJ, Zhang D, Li W, Bhattacharya M, Edelberg JM, Waldman CB, Lester SJ, Wang A, Ho CY, Jacoby D (2020). Mavacamten for treatment of symptomatic obstructive hypertrophic cardiomyopathy (EXPLORER-HCM): a randomised, double-blind, placebo-controlled, phase 3 trial. The Lancet, 396(10253), 759-769.

Mavacamten negative inotropic action is likely mediated by the shift of detached motor heads towards auto inhibited SRX state. The drug reduces peak twitch tension of intact human ventricular muscle without major changes in the time course of the twitch (unpublished). The impact of Mavacamten on cardiomyocyte electrophysiology and Ca^{2+} handling is still under investigation, but the drug is able to reverse the adverse remodelling of cardiomyocyte excitation-contraction coupling observed in mouse models of HCM[20].

The effect of increased tension in HCM can be attenuated by mavacamten action on the level of crossbridge cycle, specifically by modulation of the state transition rates between the parked state and disordered myosin detached states, capable of binding to actin. The model parameters for the change of these rates are obtained from MUSICO fits of force in HCM cardiac muscles in absence or in presence of 1 μm mavacamten (Figure 4). Parameters used for MUSICO simulations are the same as for HCM simulations from Table 3, except the parameter shown in Table 5. Using the same calcium transient as observed in HCM, and crossbridge parameters without and with mavacamten showed significant decrease in tension, ~30% for steady state force development at high [Ca^{2+}] and about 50% in twitch contractions (Figure 4 B and C). Furthermore, simulations also showed significant decrease in resting tension (Figure 4.C). These changes are similar to the tension responses as predicted by disopyramide but the mechanisms of the action of these two distinctive drugs are fundamentally different. These data show flexibility of MUSICO platform to quantitatively predict distinctively different mechanisms of drugs for the treatment of HCM patients.

Similarly, as in the previous section, the MUSICO simulations are approximately replicated by surrogate model and the surrogate fitted parameters are shown in Table 6. These data are suitable for FE analysis, i.e., for simulations of the whole heart using PAK and Alya solvers to quantitatively assess the effect of mavacamten on cardiac output including decrease in both systolic and diastolic pressures, and the ejection fraction.

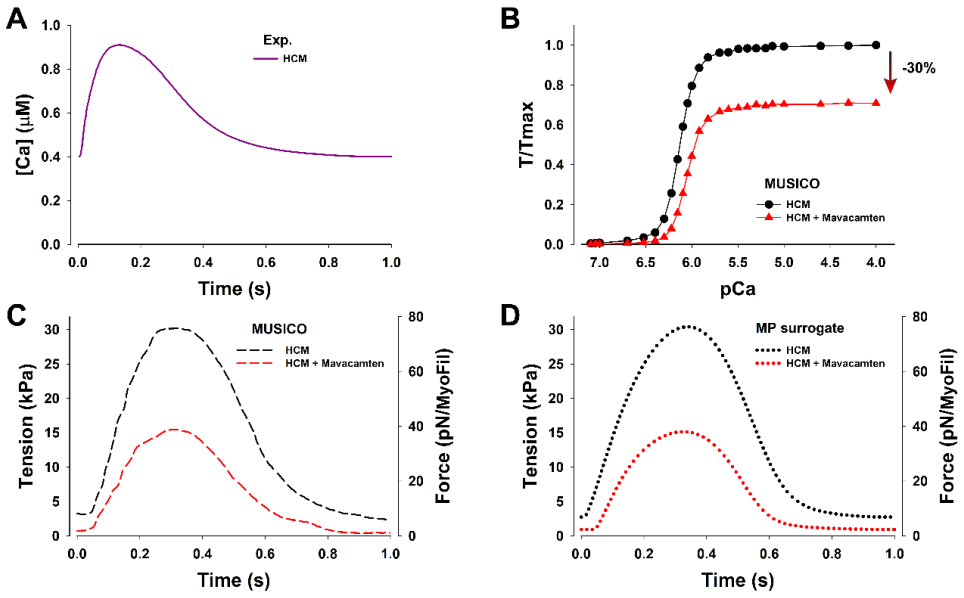

Figure 4. Mavacamten effects on twitch contraction. A) Calcium transient predictions for HCM. B) Normalized tension-pCa curves in presence of 1μM mavacamten (red) and in absence of mavacamten (black) showing 30% decrease in tension at high [Ca^{2+}]. C) MUSICO (*dashed lines*) and D) MP surrogate model (dotted lines) predictions of twitches for DCM sarcomere in presence (red) and absence mavacamten (black).

[20] Sparrow, A. J., Watkins, H., Daniels, M. J., Redwood, C., & Robinson, P. (2020). Mavacamten rescues increased myofilament calcium sensitivity and dysregulation of Ca2+ flux caused by thin filament hypertrophic cardiomyopathy mutations. American Journal of Physiology-Heart and Circulatory Physiology, 318(3), H715-H722.

Table 5. MUSICO parameters which are different from Table 3 in the presence of 1μM mavacamten

Description	Parameter	HCM	Mavacamten
Transition rate to "parked state"	k_{-PS}	200 s^{-1}	700 s^{-1}

Table 6. Parameter values for MP surrogate model for the prediction of the effect of mavacamten on HCM

Parameter	HCM	Mavacamten
SL_0	1.6	1.6
SL_isom	2.2	2.2
LA	1.1	1.1
LM	1.6	1.6
B	0.176	0.176
R_T_0	1.62E+05	$1.62 \cdot 10^5$
x0	0.007	0.007
Ca_50	0.915	0.915
k_on_0	0	0
k_on_Ca	553.70	553.70
k_off_0	100	100
k_off_Ca	150	150
k_lambda_on_0	4200	4200
k_lambda_off_0	375	375
f_0_p	512.22	187.16
h_0	357.72	973.10
h_0_p	2134.23	2495.56
g_0	173.80	369.48
k_PS_0	0.369	1.843
k_PS_max	3593.58	2954.53
b_param	5	5
Ca_50_PS	1.03	1.212
u	2.357	0.658
w	4.232	3.577
v	3.455	2.800
beta	0	0
eta	0.380	0.095
sigma_p	7.2	7.2

sigma_n	1	1
Stiff_Eq_P1	197.54	197.54
Stiff_Eq_P2	3434.96	3434.96
Stiff_Eq_P3	0	0

2.2.2 2-deoxy adenosine triphosphate (dATP)

Heart failure is the number one cause of mortality and morbidity in the developed countries and is a growing epidemic. Despite advancements in palliative treatment, the five-year mortality rate is 50%. Half of the patients suffering from heart failure have greatly reduced systolic function, yet current inotropic agents that increase contractility via increasing intracellular Ca^{2+} do not improve heart failure patient survival. Hence, there is an urgent need to develop novel agents that improve contractility and systolic function. Recently, focus has been placed on direct targeting of myofilaments to alter contractility at the level of the sarcomere and motor proteins.

The molecule 2-deoxy adenosine triphosphate (dATP) can replace ATP as the energy source for the motor protein myosin contraction in striated muscle[21,22,]. dATP allosterically enhances myosin crossbridge binding to actin (and cycling kinetic) such that small amounts of dATP are potent[23,24]. Increasing the cardiomyocyte level of dATP from the typical <0.1% of the ATP pool to just 1% is enough to significantly increase contraction[25]. A novel approach to elevate dATP *in vivo* has been developed via increasing the expression of the enzyme ribonucleotide reductase (R1R2), the rate-limiting step in de novo dNTP biosynthesis. Through either viral vector or transgenic approaches this results in increased dATP levels sufficient to increase contractile magnitude and kinetics[25]. In rodent and pig models of myocardial infarct and heart failure this therapy improves left ventricular function, including developed systolic pressure, the rate of pressure development and the rate of pressure decline at the end of systole[26]. It has been also demonstrated that dATP increases contractility of cardiac tissue from heart failure patients[27]. Thus, approaches to increase cardiomyocytes dATP constitute an exciting and novel therapy with the potential to treat heart failure.

The significant increase in cardiac muscle contractility could be beneficial for DCM cardiomyopathies. Using MUSICO simulations, we quantitatively assessed the effect of dATP as the energy source on twitch contractions in mice trabeculae stimulated with frequency of 1Hz at 30°C. A comparison of the experimental twitch responses in intact (mouse) trabeculae between transduced probes by R1R2 enzyme expressing ~1.5 [dATP] of adenine nucleotide content[25] (denoted as dATP) and WT that

[21] M. Regnier, D.M. Lee, E. Homsher, ATP analogs and muscle contraction: mechanics and kinetics of nucleoside triphosphate binding and hydrolysis, Biophys J 74(6) (1998) 3044-58.
[22] M. Regnier, A.J. Rivera, Y. Chen, P.B. Chase, 2-deoxy-ATP enhances contractility of rat cardiac muscle, Circ Res 86(12) (2000) 1211-7.
[23] M. Regnier, E. Homsher, The effect of ATP analogs on posthydrolytic and force development steps in skinned skeletal muscle fibers, Biophys J 74(6) (1998) 3059-71.
[24] M. Regnier, H. Martin, R.J. Barsotti, A.J. Rivera, D.A. Martyn, E. Clemmens, Cross-bridge versus thin filament contributions to the level and rate of force development in cardiac muscle, Biophys J 87(3) (2004) 1815-24.
[25] F.S. Korte, J. Dai, K. Buckley, E.R. Feest, N. Adamek, M.A. Geeves, C.E. Murry, M. Regnier, Upregulation of cardiomyocyte ribonucleotide reductase increases intracellular 2 deoxy-ATP, contractility, and relaxation, J Mol Cell Cardiol 51(6) (2011) 894-901.
[26] S.G. Nowakowski, S.C. Kolwicz, F.S. Korte, Z. Luo, J.N. Robinson-Hamm, J.L. Page, F. Brozovich, R.S. Weiss, R. Tian, C.E. Murry, M. Regnier, Transgenic overexpression of ribonucleotide reductase improves cardiac performance, Proc Natl Acad Sci U S A 110(15) (2013) 6187-92.
[27] F. Moussavi-Harami, M.V. Razumova, A.W. Racca, Y. Cheng, A. Stempien-Otero, M. Regnier, 2-Deoxy adenosine triphosphate improves contraction in human end-stage heart failure, J Mol Cell Cardiol 79 (2015) 256-63.

express < 0.2% [dATP] (denoted as ATP), and the predictions by MUSICO and MP surrogate model are shown in Figure 5. Since the experimental intracellular calcium was not measured, we used the same calcium transient, derived from the observations of Davis et al.[28], in both cases for MUSICO and MP surrogate model simulations.

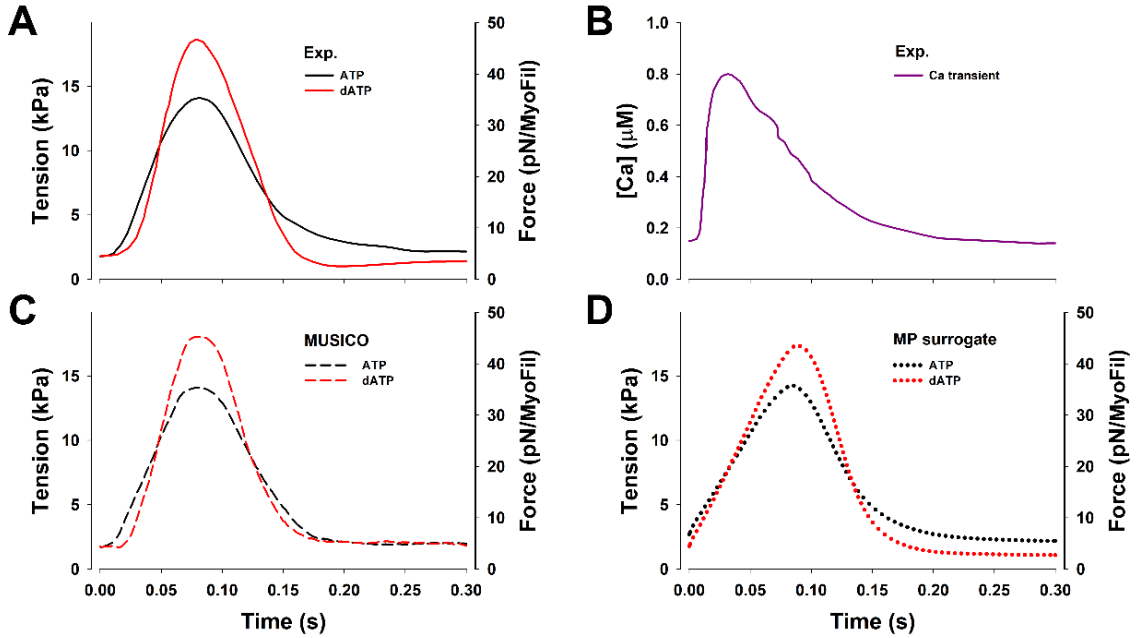

Figure 5.MUSICO (*dashed lines*) and MP surrogate model (dotted lines) predictions of twitches by using ATP and dATP as the energy source in mice trabeculae at 30° C superimposed on the observed twitches (*solid lines*). The twitches are driven by the same Ca^{2+} transients (inset).

Differences in estimated MUSICO parameters (Table 7) are only in myosin-actin binding and detachment rates, k_{+A} and k_{-A} respectively, while keeping the equilibrium binding rate constant, and k_{+D}, resulting in higher force generation and faster rise and relaxation times. Parameter values for MP surrogate model are shown in Table 8.

Table 7. MUSICO parameters for the prediction of the effect of using ATP and dATP as the energy source on twitch in mice trabeculae at 30° C

	Description	Parameter	ATP	dATP
Crossbridge Cycle	Myosin-actin binding rate	k_{+A}	220 s^{-1}	700 s^{-1}
	Myosin-actin detachment rate	k_{-A}	145 s^{-1}	460 s^{-1}
	Myosin stroke cap rate	k_{+Pi_cap}	1000 s^{-1}	1000 s^{-1}
	Myosin reverse stroke cap rate	k_{-Pi_cap}	100 s^{-1}	100 s^{-1}
	Power stroke energy	G_{stroke}	-13 k_BT	-13 k_BT
	Working stroke	d	10.5 nm	10.5 nm
	Second working stroke	δ	1 nm	1 nm
	ADP release rate	k_{+D}	200 s^{-1}	400 s^{-1}

[28] Davis, J., Davis, L. C., Correll, R. N., Makarewich, C. A., Schwanekamp, J. A., Moussavi-Harami, F., ... & Molkentin, J. D. (2016). A tension-based model distinguishes hypertrophic versus dilated cardiomyopathy. Cell, 165(5), 1147-1159.

	ATP binding and myosin detach.	k_{+T}	10^6 s^{-1}	10^6 s^{-1}
	Hydrolysis forward rate	k_{+H}	100 s^{-1}	100 s^{-1}
	Hydrolysis backward rate	k_{-H}	10 s^{-1}	10 s^{-1}
	Crossbridge stiffness	κ	1.3 pN/nm	1.3 pN/nm
	k_BT at 30°C	k_BT	4.185 pN·nm	4.185 pN·nm
Calcium Kinetics	Calcium binding to TnC equilibrium rate constant	K_{Ca}	10^6 M^{-1}	10^6 M^{-1}
	Calcium binding to TnC	$\tilde{k}_{Ca}$	$7.54{\cdot}10^7$ $M^{-1}{\cdot}s^{-1}$	$7.54{\cdot}10^7$ $M^{-1}{\cdot}s^{-1}$
	Calcium Dissociation Rate from TnC	k_{-Ca}	75.4 s^{-1}	75.4 s^{-1}
	TnI-actin equilibrium rate const. at high Ca^{2+}	λ	10	10
	TnI-actin-Ca cooperativity coefficient	ε_o	0.01	0.01
CFC	Tropomyosin pinning angle	ϕ_-	-25°	-25°
	Myosin Tm angular displ.	ϕ_+	10°	10°
	Angular SD of free CFC	σ_0	29.7°	29.7°
	Persistence length of Tm-Tn confined chain	$1/\xi$	50 nm	50 nm
Parked State	Transition rate to “parked state”	k_{-PS}	200 s^{-1}	200 s^{-1}
	Baseline rate	k_{PS}^0	5 s^{-1}	5 s^{-1}
	Amplitude	k_{PS}^{max}	400 s^{-1}	400 s^{-1}
	Hill function slope	b	5	5
	Half activation point of the Hill function	$[Ca_{50}]$	1 μM	1 μM
Sarcomere	Length of Sarcomere	SL	2.2 μM	2.2 μM
	Length of Actin fiber	L_a	1.1 μM	1.1 μM
	Thin filament elastic modulus	AE_a	65 nN	65 nN
	Thick filament elastic modulus	AE_m	132 nN	132 nN

Table 8. Parameter values for MP surrogate model for the prediction of the effect of using ATP and dATP as the energy source on twitch in mice trabeculae at 30° C

Parameter	ATP	dATP
SL_0	1.6	1.6
SL_isom	2.2	2.2
LA	1.1	1.1

LM	1.6	1.6
B	0.176	0.176
R_T_0	$1.62 \cdot 10^5$	$1.62 \cdot 10^5$
x0	0.007	0.007
Ca_50	0.915	0.915
k_on_0	0	0
k_on_Ca	406.85	406.85
k_off_0	100	100
k_off_Ca	224.03	224.03
k_lambda_on_0	3750	3750
k_lambda_off_0	375	375
f_0_p	477.46	539.95
h_0	329.59	254.98
h_0_p	1767.50	1304.48
g_0	295.99	241.31
k_PS_0	3.387	1.275
k_PS_max	1051.02	1630.15
b_param	5	5
Ca_50_PS	1	1
u	3.654	2.731
w	4.438	5.646
v	2.331	3.371
beta	0	0
eta	0.591	0.319
sigma_p	7.2	7.2
sigma_n	1	1
Stiff_Eq_P1	197.54	197.54
Stiff_Eq_P2	3434.96	3434.96
Stiff_Eq_P3	0	0

2.3 Drugs that affect changes in macroscopic parameters

The workflow for testing these types of drugs is shown in Figure 1C. The experimental observations in many clinical trials are used as an input for FE models yielding us the precise model of Entresto® action.

2.3.1 Entresto

ENTRESTO® (Sacubitril/valsartan) has been shown to be superior to enalapril in reducing the risks of death and hospitalization for heart failure (HF). There are also publications which evaluate the effects of sacubitril/valsartan on clinical, biochemical, and echocardiographic parameters in patients with heart failure and reduced ejection fraction (HFrEF).

The first-in-class angiotensin receptor neprilysin inhibitor (ARNI) sacubitril/valsartan combines the angiotensin II type-1 receptor blocker (ARB) valsartan with the neprilysin inhibitor sacubitril. Entresto® was superior to enalapril in decreasing risks of death and new admission for HF in patients with HFrEF in the Prospective Comparison of ARNI with ACEI to Determine Impact on Global Mortality and Morbidity in Heart Failure (PARADIGM-HF) study[29]. Romano et al[30], investigated the effects of sacubitril/valsartan on clinical, biochemical and echocardiographic, parameters in HFrEF patients.

They find that Entresto® can be "hemodynamic recovery" drug. A modulation of neurohormonal activation determined by this drug may lead to a hemodynamic effect that may impact cardiac hemodynamic and in association with Nt-proBNP concentration abatement could lead to a ameliorate NYHA (New York Heart Association) class and reduce diuretics administration and consequently to preserve renal function.

Entresto® reduced E/A ratio, MR, TR velocity and Nt-ProBNP concentration. This hemodynamic effect ameliorates the NYHA class and reduce diuretic dose at follow-up. MR, mitral regurgitation from moderate to severe grade; E/A: peak e-wave velocity/ peak a-wave velocity ratio; TR velocity: tricuspid regurgitation peak velocity (Figure 6.).

For example, the main Entresto® component, valsartan, strongly interacts with Angiotensin II receptor inducing the left ventricular hypertrophy in patients with essential hypertension. Left ventricular hypertrophy (LVH) represents an independent risk factor in patients with essential hypertension. In a randomized, double-blind trial, 69 predominantly previously untreated hypertensive patients with echocardiographically proven LVH, i.e., left ventricular mass index (LVMI) >134 g/m^2 in men and >110 g/m^2 in women and/or end-diastolic septal thickness >12 mm, received the angiotensin II antagonist valsartan for 8 months[31]. The study revealed that the dose of 80 mg/day decreased LVMI from 125 to 105 g/m^2 in 8 months. End-diastolic posterior and end-diastolic septal wall thickness also significantly decreased. Left ventricular end-diastolic and end-systolic diameter also decreased.

[29] McMurray, J. J., Packer, M., Desai, A. S., Gong, J., Lefkowitz, M. P., Rizkala, A. R., Rouleau, J.L., Shi, V.C., Solomon, S.D., Swedberg, K. & Zile, M. R. (2014). Angiotensin–neprilysin inhibition versus enalapril in heart failure. N Engl J Med, 371, 993-1004.

[30]Romano, G., Vitale, G., Ajello, L., Agnese, V., Bellavia, D., Caccamo, G., ... & Clemenza, F. (2019). The effects of sacubitril/valsartan on clinical, biochemical and echocardiographic parameters in patients with heart failure with reduced ejection fraction: the "hemodynamic recovery". Journal of clinical medicine, 8(12), 2165.

[31] Thürmann, P. A., Kenedi, P., Schmidt, A., Harder, S., & Rietbrock, N. (1998). Influence of the angiotensin II antagonist valsartan on left ventricular hypertrophy in patients with essential hypertension. Circulation, 98(19), 2037-2042.

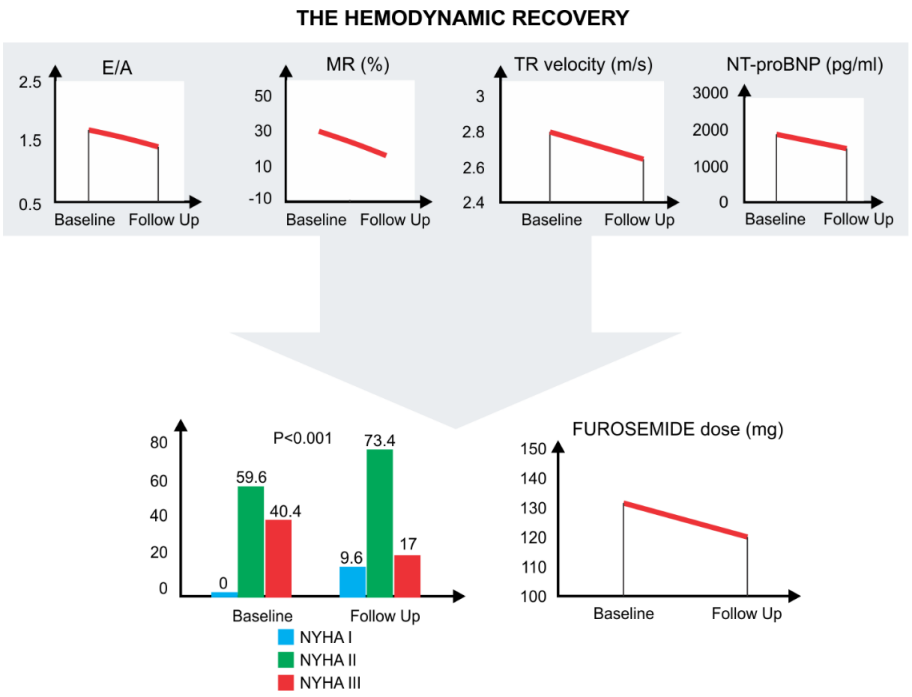

Figure 6. Hemodynamic recovery

The influence of valsartan predominantly indicated significant increase in left ventricular end-diastolic and end-systolic volume, while ejection fraction remained in the same boundaries (Table 9).

Table 9. Influence of 80 mg/day dose of Entresto®

Parameter	0 months	8 months
LVMI –left ventricular mass index,	125 g/m^2	105 g/m^2
PWTd - end-diastolic posterior wall thickness	13.6 ± 0.7 mm	12.4 ± 1.0 mm
IVSd - end-diastolic septal wall thickness	13.7 ± 1.2 mm	12.2 ± 1.1 mm
LVIDd - left ventricular end-diastolic diameter	47.24 ± 5.13 mm	46.22 ± 5.54 mm
LVIDs - left ventricular end-systolic diameter	29.07 ± 4.83 mm	28.46 ± 4.15 mm
FS - fractional shortening	39 ± 8 %	38 ± 6 %
LVEDV - left ventricular end-diastolic volume	91.00 ± 27.38 mL	94.97 ± 21.94 mL
LVESV - left ventricular end-systolic volume	31.31 ± 15.67 mL	34.07 ± 11.59 mL
EF - ejection fraction	65 ± 10 %	65 ± 7 %

Table 10 shows observed changes for Doppler echocardiographic parameters.

Table 10. Doppler Echocardiographic Parameters

Parameter	0 months	8 months
$V_{max}E$, maximal velocity of early diastolic filling phase	75.30 ± 18.27 cm/s	70.14 ± 12.42 cm/s
$V_{max}A$, maximal velocity of late diastolic filling phase	82.64 ± 19.35 cm/s	78.07 ± 16.48 cm/s
∫E, time/velocity integral of early diastolic filling phase	10.76 ± 3.02 cm	11.61 ± 2.33 cm
∫A, time/velocity integral of late diastolic filling phase	10.66 ± 2.98 cm	10.46 ± 2.60 cm
∫E/∫A	1.06 ± 0.33	1.16 ± 0.29

2.3.2 Disopyramide Macro Change

In addition to the fact that disopyramide acts as a sodium channel blocker and thus significantly affects Ca^{2+} homeostasis in human HCM disease, it also affects macroscopic parameters. Disopyramide is a class Ia antiarrhythmic that is used for the treatment from 1977. However, disopyramide is also employed because of its solid negative inotropic effect by reducing the inward sodium current of the cardiomyocyte through phase 0 of the action potential, reaching a considerable reduction of its upstroke velocity. Clinical studies have shown significant advancements in heart failure indications and a decrease in the requirement for invasive therapy in patients cured with disopyramide. Disopyramide, has been shown to slow speeding up of LV ejection flow and extend flow acceleration time, which postpone or eliminates mitral–septal contact[32]. In pharmacodynamic studies, disopyramide significantly reduces both resting and provoked left ventricular outflow tract obstruction gradient[33].

Disopyramide has shown an impact on many parameters of heart tissue. Clinical trials proved shortening of left ventricle and interventricular septum (Table 11). On the other hand, disopyramide induces significant increase in posterior wall thickness[34] (Table 12). 100 mg of disopyramide significantly increases heart rate, aortic pressure and epicardial arterial diameter with contraction of left ventricle pressure[35] and ejection fraction percentage[36] (Table 13 and Table 14). On the other hand, disopyramide significantly induces the increase of heartbeat values, epicardial arterial diameter SBP and DBP in acute fashion (Tables 7-10).

Table 11. Effect of Disopyramide on Left Ventricular Standard Dimensions

Time	LV, cm		IVS, cm		PW, cm		FS, %
	d	s	d	s	d	s	
Control	5.06 ± 0.26	3.51 ± 0.19	0.86 ± 0.10	1.18 ± 0.12	0.89 ± 0.14	1.59 ± 0.20	30.60 ± 1.70
5 min	5.21 ± 0.24	3.93 ± 0.21	0.74 ± 0.20	1.10 ± 0.14	0.89 ± 0.17	1.42 ± 0.18	24.40 ± 2.70
15 min	5.12 ± 0.20	3.99 ± 0.28	0.76 ± 0.21	1.03 ± 0.14	0.94 ± 0.15	1.40 ± 0.18	22.00 ± 3.50
60 min	4.86 ± 1.14	3.76 ± 0.18	0.77 ± 0.22	1.07 ± 0.15	0.95 ± 1.14	1.51 ± 0.20	26.6 ± 2.80

where:

- d – diastole
- s – systole
- LV – left ventricle
- IVS – interventricular septum

[32] Sherrid, M. V., Pearle, G., & Gunsburg, D. Z. (1998). Mechanism of benefit of negative inotropes in obstructive hypertrophic cardiomyopathy. Circulation, 97(1), 41-47.

[33] Kimball, B. P., Bui, S., & Wigle, E. D. (1993). Acute dose-response effects of intravenous disopyramide in hypertrophic obstructive cardiomyopathy. American heart journal, 125(6), 1691-1697.

[34] Pollick, C., Giacomini, K. M., Blaschke, T. F., Nelson, W. L., Turner-Tamiyasu, K., Briskin, V. & Popp, R. L. (1982). The cardiac effects of d-and l-disopyramide in normal subjects: a noninvasive study. Circulation, 66(2), 447-453.

[35] Hongo, M., Nakatsuka, T., Takenaka, H., Tanaka, M., Watanabe, N., Yazaki, Y., & Sekiguchi, M. (1996). Effects of intravenous disopyramide on coronary hemodynamics and vasodilator reserve in hypertrophic obstructive cardiomyopathy. Cardiology, 87(1), 6-11.

[36] Hartmann, A., Kühn, J., Hopf, R., Klepzig, H., Standke, R., Kober, G., ... & Kaltenbach, M. (1992). Effect of propranolol and disopyramide on left ventricular function at rest and during exercise in hypertrophic cardiomyopathy. Cardiology, 80(2), 81-88.

- PW – posterior wall
- FS – fractional shortening of LV

Table 12. Effect of Disopyramide on Heart Rate and Blood Pressure

Time	Heart Rate (beats/min)	SBP, mm Hg	DBP, mm Hg
Control	58.00 ± 6.00	117.00 ± 11.00	77.00 ± 8.00
5 min	54.00 ± 7.00	116.00 ± 8.00	83.00 ± 6.00
15 min	61.00 ± 7.00	116.00 ± 10.00	86.00 ± 7.00
60 min	59.00 ± 6.00	119.00 ± 9.00	86.00 ± 7.00

Table 13. Effects of disopyramide on clinical and echocardiographic features in patients with HCM

		Disopyramide	
	Control, 0 mg	**50 mg**	**100 mg**
Heart Rate, b/min	64 ± 11	62 ± 12	67 ± 10
LVP, mm Hg	177 ± 31	160 ± 26	146 ± 23
Aortic pressure, mm Hg	123 ± 23	130 ± 25	135 ± 25
Epicardial arterial diameter, mm	3.5 ± 0.6	3.9 ± 0.5	4.1 ± 0.6

Table 14. Effects of disopyramide on left ventricular systolic and diastolic function at rest and during exercise

		HR, bpm	EF, %
Control	Rest	73 ± 21	72 ± 12
	Exercise	121 ± 21	76 ± 9
Disopyramide (acute treatment)	Rest	75 ± 21	71 ± 11
	Exercise	124 ± 24	74 ± 12
Disopyramide (long-term treatment)	Rest	76 ± 21	69 ± 14
	Exercise	120 ± 19	76 ± 12

2.3.3 Digoxin Macro Change

Digoxin is proven to enhance hemodynamic responses in heart failure and regulation of heart rate in atrial fibrillation. Digoxin was FDA approved since 1997 for improving symptoms and decreasing the risk of heart failure-related hospitalizations and emergency care in patients with heart failure and for controlling ventricular rate in patients with chronic atrial fibrillation[37]. Digoxin lowers the threat of the primary composite outcome in patients with heart failure with reduced ejection fraction. It has been greatly utilized when handling a number of heart difficulties, including congestive heart failure, atrial fibrillation or flutter, and particular cardiac arrhythmias. It operates by improving myocardial contractility, rising stroke volume and blood pressure, lowering heart rate, rather than broadening the timeframe of a contraction. It can cause an improvement of myocardial function and hemodynamics,

[37] The U.S. Food and Drug Administration. Digoxin Products for Oral Use; Reaffirmation of New Drug Status and Conditions for Marketing. In: Federal Register (The Daily Journal of the United States Government), ed. Vol 65 65 FR 70573. Washington, DC: Department of Health and Human Services (HHS); 2000:70573-70575

in conjunction with increased perfusion of tissues. Digoxin has two principal mechanisms of action which are selectively employed varying on the indication[38]:

- Positive Ionotropic: It raises the strength of contraction of the heart by reversibly constraining the activity of the myocardial Na-K ATPase pump, an enzyme that regulates the flow of ions into the heart. Digoxin generates a rise in intracellular sodium that will lead to an influx of calcium in the heart and produce an enhancement in contractility. Cardiac output improves with a following reduction in ventricular filling pressures.
- AV Node Inhibition: Digoxin has vagomimetic effects on the AV node. By promoting the parasympathetic nervous system, it decelerates electrical transmission in the atrioventricular node, hence, reduces the heart rate. The increase in calcium concentrations indicates continuation of phase 4, and phase 0 of the cardiac action potential therefore rises the refractory period of the AV node. Slower transmission through the AV node brings a reduced ventricular response.

Similarly to Entresto, Digoxin is one of the key drugs in cardiomyopathy treatment. Median dosage of digoxin (0.25 mg) induced a slightly decrease in right atrial length (apical view)[39], while the left ventricular end-diastolic and end-systolic diameter significantly decreased (Table 15). Digoxin induced no significant change in septal and posterior wall thickness and in ejection fraction. Another study described lowering of heart rate and shortening of the left ventricular dimension in basal and overloading pressure conditions[40] (Table 16 and Table 17).

Table 15. Baseline characteristics of patients treated with or without digoxin

Parameter	No digoxin	Digoxin
Left atrial size, long axis – mm	46±6	46±7
Right atrial length, apical view – mm	59±8	57±8
Left ventricular end diastolic diameter – mm	50±7	52±8
Left ventricular end systolic diameter – mm	35±8	37±9
Septal thickness – mm	11±2	11±2
Posterior wall thickness – mm	10±2	10±2
Left ventricular ejection fraction – mean±SD – %	52±10	52±13
Left ventricular ejection fraction ≤40% – no. (%)	40	51

Table 16. Echocardiographic Parameters – Basal

Parameter	No digoxin	Digoxin
Heart Rate (beats/min)	67	62
Systolic Blood Pressure (mm Hg)	107	111
EF (%)	74	79

[38] Ren, Y., Ribas, H. T., Heath, K., Wu, S., Ren, J., Shriwas, P., ... & Kinghorn, A. D. (2020). Na+/K+-ATPase-Targeted Cytotoxicity of (+)-Digoxin and Several Semisynthetic Derivatives. Journal of natural products, 83(3), 638-648.
[39] Mulder, B. A., Van Veldhuisen, D. J., Crijns, H. J., Tijssen, J. G., Hillege, H. L., Alings, M., ... & RACE II Investigators. (2014). Digoxin in patients with permanent atrial fibrillation: data from the RACE II study. Heart Rhythm, 11(9), 1543-1550.
[40] Crawford, M. H., Karliner, J. S., & O'Rourke, R. A. (1976). Favorable effects of oral maintenance digoxin therapy on left ventricular performance in normal subjects: echocardiographic study. The American journal of cardiology, 38(7), 843-847.

Percent shortening of the left ventricular dimension	37	41
Rate of left ventricular dimension shortening	5.66 ± 0.22	6.31 ± 0.23

Table 17. Echocardiographic Parameters – During pressure overloading

Parameter	No digoxin	Digoxin
Heart Rate (beats/min)	93	97
Systolic Blood Pressure (mm Hg)	153	156
EF (%)	69	75
Percent shortening of the left ventricular dimension	33	38
Rate of left ventricular dimension shortening	5.46 ± 0.32	6.48 ± 0.33

2.3.4 Mavacamten Macro Change

Mavacamten is a first-in-class targeted inhibitor of cardiac myosin, which has been shown to reduce LV outflow tract obstruction, improve exercise capacity, and relieve cardiomyopathy symptoms. The main action mechanism is the reduction of actin–myosin cross-bridge formation, and inhibition of sarcomere force production, thereby reducing contractility. Initial mechanistic studies have suggested that mavacamten primarily reduces the steady-state ATPase activity by inhibiting the rate of phosphate release of -cardiac myosinS1, but the molecular mechanism of action of mavacamten has not been described[41]. This, in turn, reduces the inotropic force and may also facilitate diastolic relaxation. Mavacamten is, therefore, predicted to improve both diastolic dysfunction and relieve left ventricular outflow tract obstruction in patients with HCM. In mouse studies, early treatment of phenotype negative HCM mice prevented development of hypertrophy and other hallmarks of HCM; administration to mice with the HCM phenotype attenuated hypertrophic and profibrotic gene expression as well[18].

A new phase 3 trial study revealed the influence of mavacamten in treatment of cardiomyopathy. Diastolic blood pressure decreased in the mavacamten group, compared to placebo group[19] (Table 18). Left ventricular ejection fraction, left atrial diameter and maximum left ventricular wall thickness did not show any significant change[42] (Table 19).

Table 18. Characteristics for Placebo and Mavacamten group

[41] Kawas, R. F., Anderson, R. L., Ingle, S. R. B., Song, Y., Sran, A. S., & Rodriguez, H. M. (2017). A small-molecule modulator of cardiac myosin acts on multiple stages of the myosin chemomechanical cycle. Journal of Biological Chemistry, 292(40), 16571-16577.

[42] Ho, C. Y., Mealiffe, M. E., Bach, R. G., Bhattacharya, M., Choudhury, L., Edelberg, J. M., ... & Heitner, S. B. (2020). Evaluation of mavacamten in symptomatic patients with nonobstructive hypertrophic cardiomyopathy. Journal of the American College of Cardiology, 75(21), 2649-2660.

	Placebo group	Mavacamten group
DBP, mm Hg	76	75
LVEF, %	74	74
Maximum left ventricular wall thickness, mm	20	20
Left atrial volume index, mL/m²	41	40
Left atrial diameter, mm	42	42

Table 19. Baseline characteristics – Mavacamten

	Placebo group	Mavacamten group 200 ng/ml	Mavacamten group 500 ng/ml
Maximal LV wall thickness, mm	18.8 ± 3.5	20.9 ± 3.0	20.4 ± 4.8
LVEF, %	66.4 ± 7.7	68.0 ± 5.2	69.4 ± 5.8
Left ventricular end-diastolic volume, mL	60.5 ± 21.6	59.5 ± 14.5	58.5 ± 18.6

3. Using PAK and ECG modules for drug testing

3.1 Different scenarios for PAK Solver Tool

3.1.1 Basic geometry

In this chapter we will show the results obtained with our parametric model and describe how PV diagrams depend on the change of Ca2+, elasticity of the wall and the inlet and outlet velocity profile. This directly affects the ejection fraction. Basic geometry is shown in Figure 7, and standard inlet and outlet velocities are shown in Figure 8.

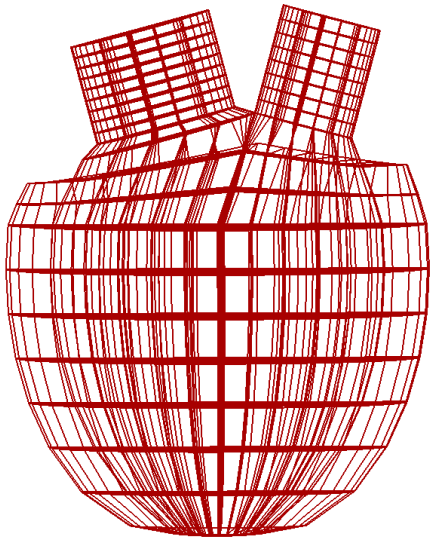

Figure 7. Basic geometry of left ventricle parametric model

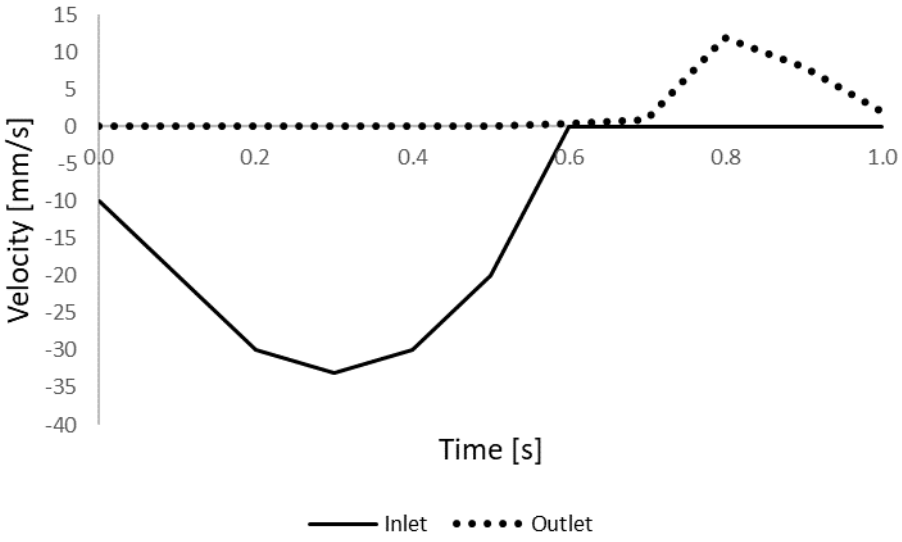

Figure 8. Prescribed inlet and outlet velocities for aortic output and mitral input

Displacement field at 0.2s, 0.5s and 0.6s is shown in Figure 9. Velocity field at 0.2s, 0.5s and 0.6s is shown in Figure 10. Pressure field at 0.2s, 0.5s and 0.6s is shown in Figure 11.

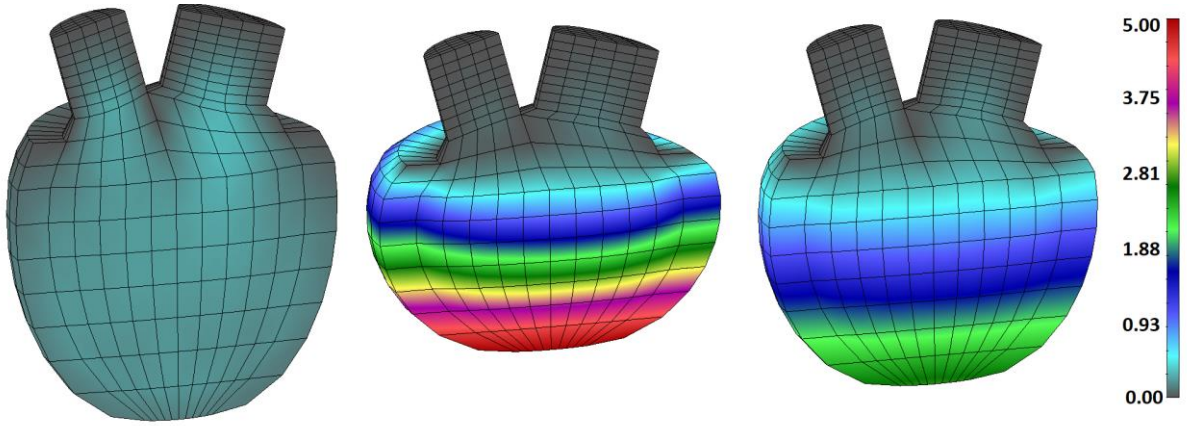

Figure 9. Displacement field at 0.2s, 0.5s and 0.6s for parabolic Ca^{2+} concentration function

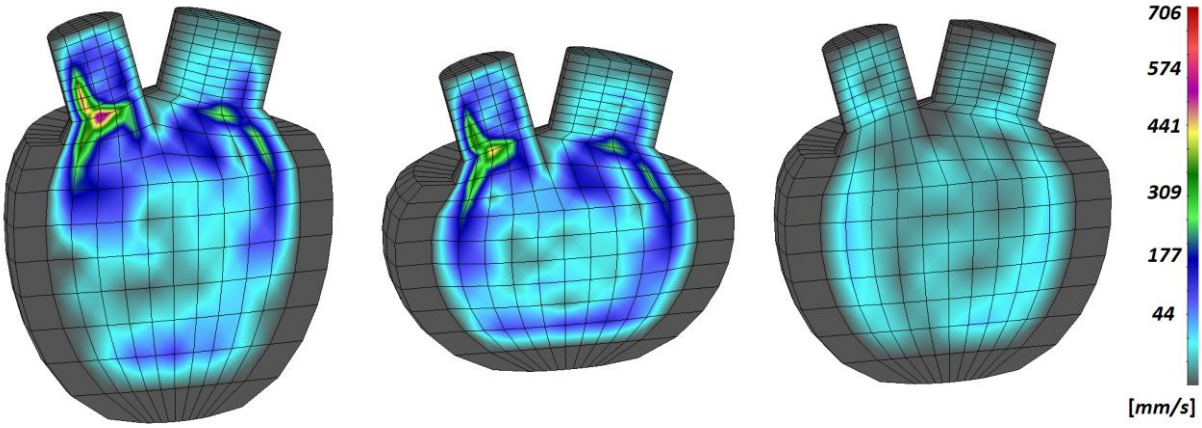

Figure 10. Velocity field at 0.2s, 0.5s and 0.6s for parabolic Ca^{2+} concentration function

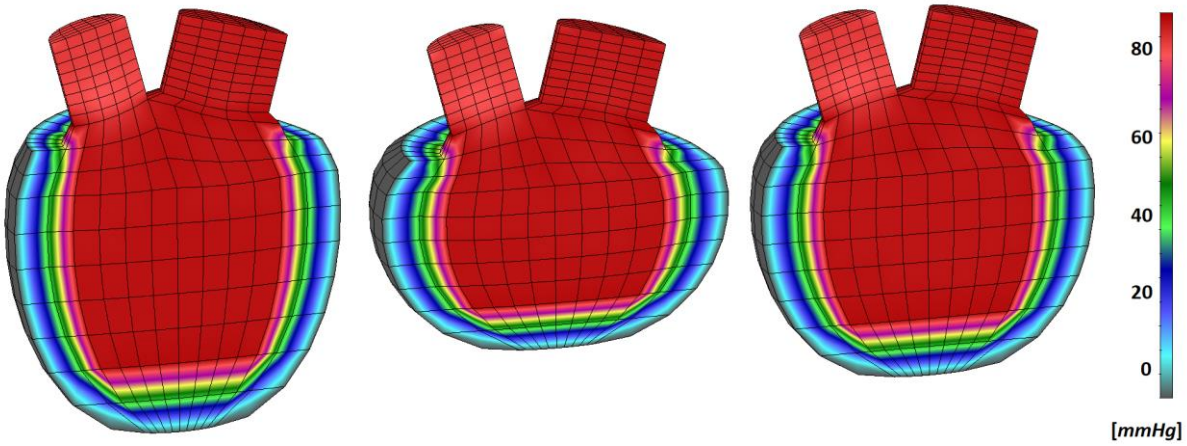

Figure 11. Pressure field at 0.2s, 0.5s and 0.6s for parabolic Ca^{2+} concentration function

Effect of different Ca2+ concentration functions to the ejection fraction of LV is shown in Figure 12.

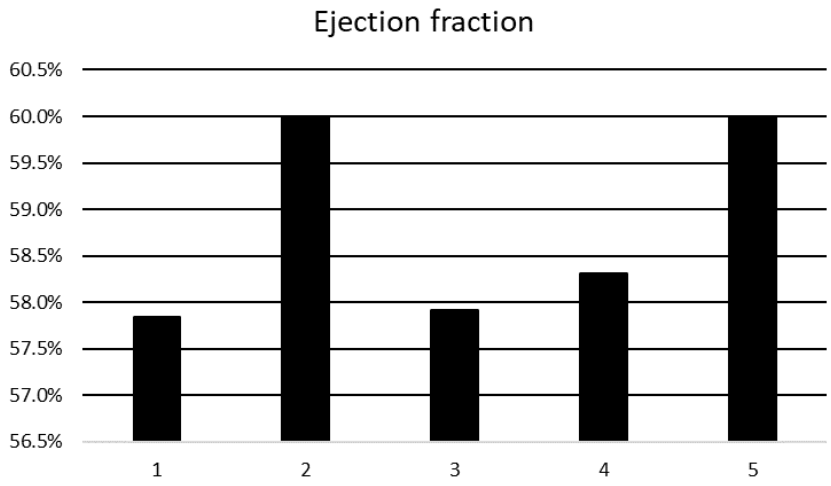

Figure 12. Ejection fraction of LV for (1) triangular, (2) parabolic, (3) steep, (4) shifted parabolic and (5) parabolic wider Ca2+ concentration function

3.1.2 Scenario 1a: Influence of Holzapfel scale factor (elasticity)

In this section, we will examine the influence of elasticity on the cardiac cycle. PV diagrams for 20% higher and 20% lower elasticity are shown in Figure 13. PV diagrams for 30% higher and 50% lower elasticity are shown in Figure 14. The effect of the elasticity on the ejection fraction is shown in Figure 15.

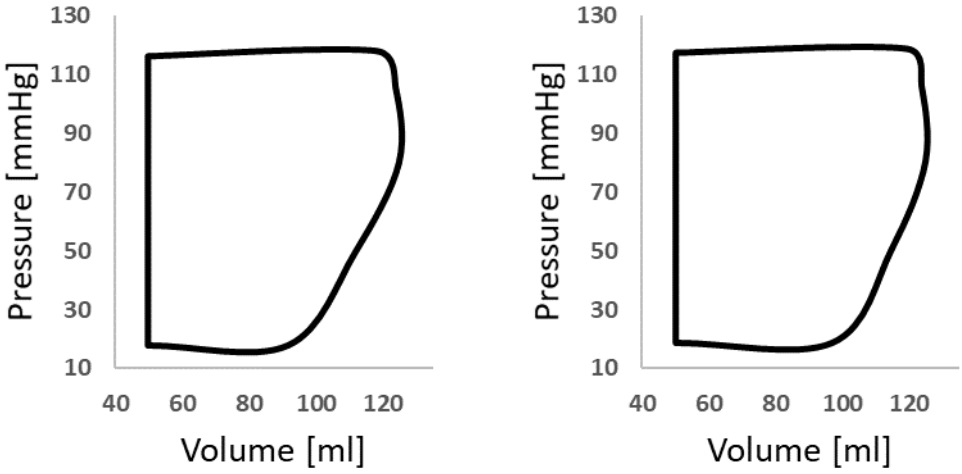

Figure 13. PV diagrams for 20 % higher (left) and 20% lower (right) elasticity

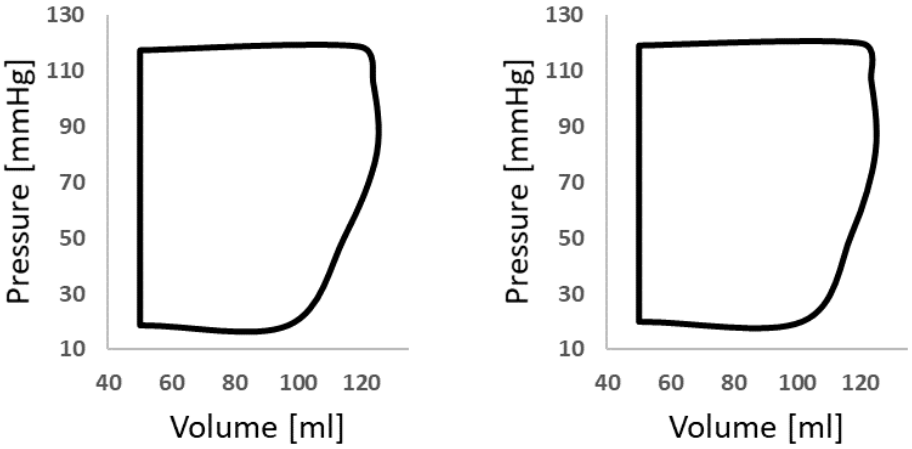

Figure 14. PV diagrams for 30 % higher (left) and 50% lower (right) elasticity

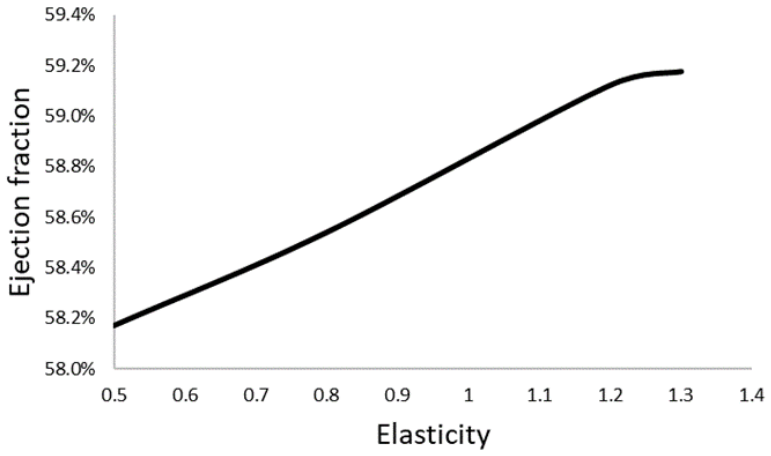

Figure 15. Effect of the elasticity to the ejection fraction

3.1.3 Scenario 2a: Influence of inlet and outlet velocities

In this section, we will examine the influence of inlet and outlet velocities on the cardiac cycle. PV diagrams for 25% higher inlet velocities and 25% higher outlet velocities are shown in Figure 16.

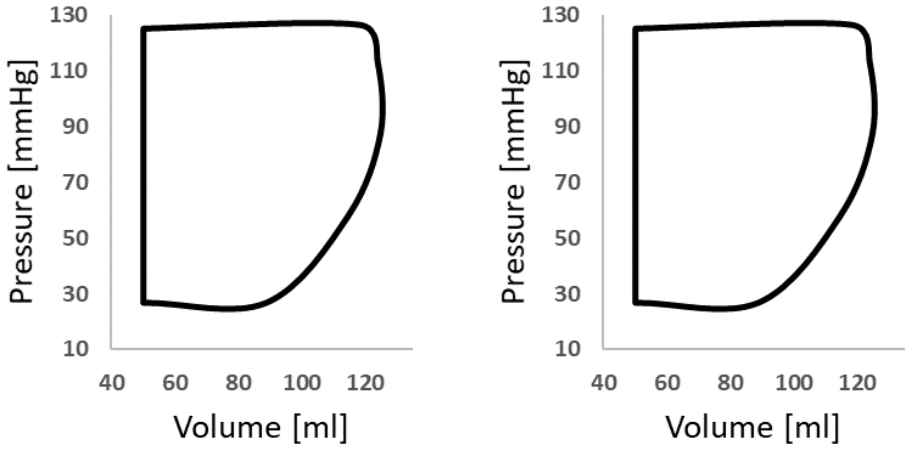

Figure 16. PV diagrams for Inlet velocity from the left atrium 25% higher (left) and outlet velocity 25% higher (right)

PV diagrams for 25% lower inlet velocity and 25% lower outlet velocity are shown in Figure 17. PV diagrams for the scenario with 30% higher inlet and the scenario with 30% higher outlet velocity are shown in Figure 18. PV diagrams for the scenario with 50% lower inlet velocity and the scenario with 50% lower outlet velocity are shown in Figure 19. In Figure 20, we present the effect of inlet velocity on ejection fraction. In Figure 21, we show the effect of outlet velocity on ejection fraction.

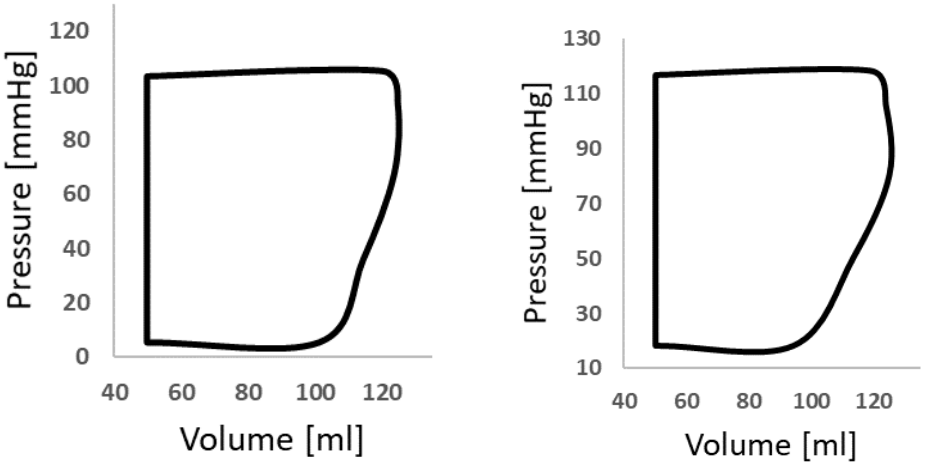

Figure 17. PV diagrams for Inlet velocity from the left atrium 25% lower (left) and outlet velocity 25% lower (right)

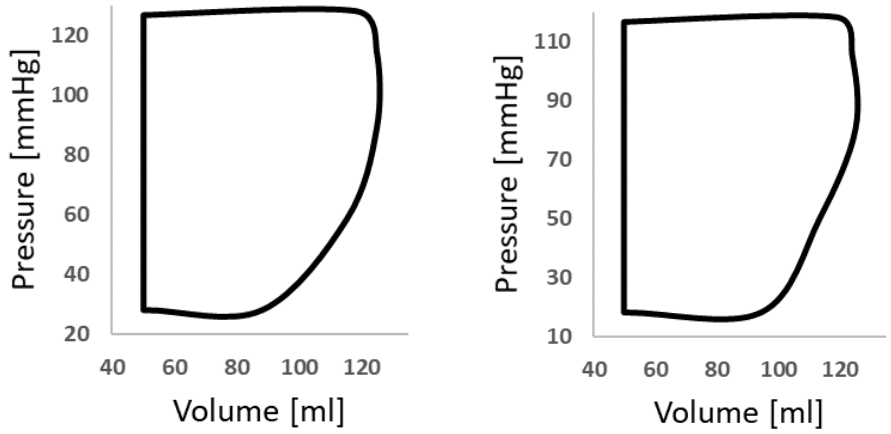

Figure 18. PV diagrams for Inlet velocity from the left atrium 30% higher (left) and outlet velocity 30% higher (right)

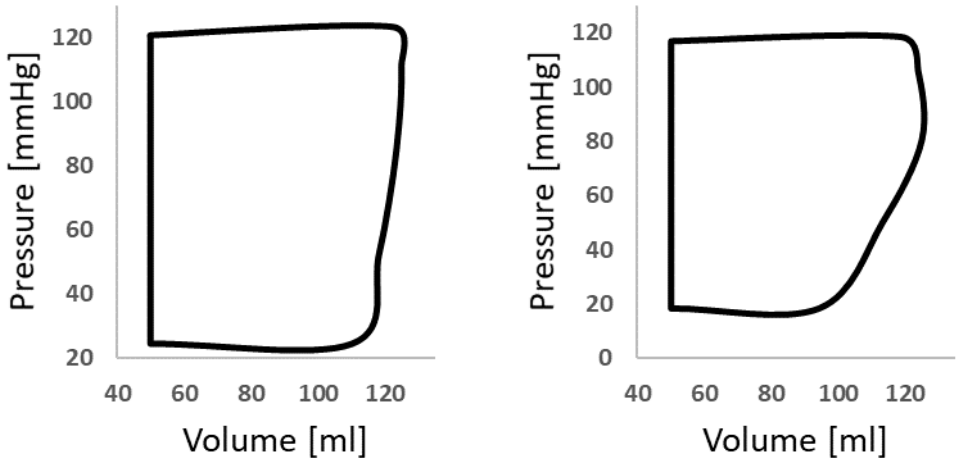

Figure 19. PV diagrams for outlet velocity from the left atrium 50% lower (left) and input velocity 50% lower (right)

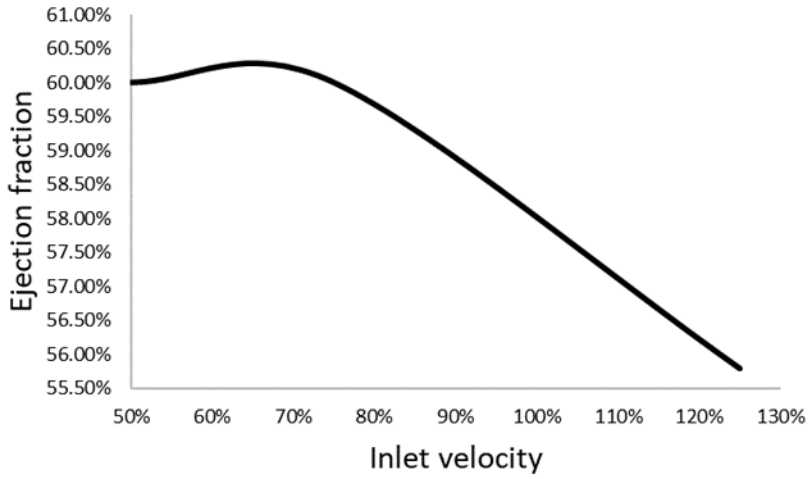

Figure 20. Ejection fraction with respect to inlet velocity

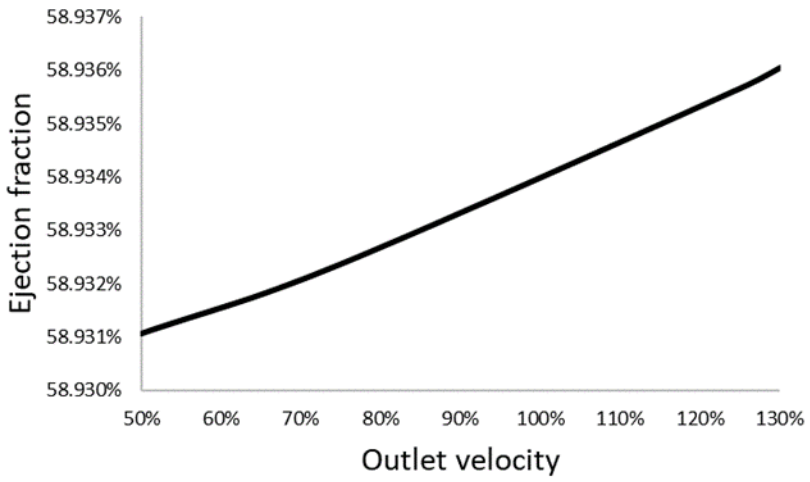

Figure 21. Ejection fraction with respect to outlet velocity

3.1.4 Scenario 3a: Influence of Ca^{2+} concentration

Triangular Ca^{2+} concentration function is shown in Figure 22 along with the corresponding PV diagram. Parabolic Ca2+ concentration function and the corresponding PV diagram are shown in Figure 23. Steep Ca2+ concentration function and the corresponding PV diagram are shown in Figure 24. Shifted parabolic Ca2+ concentration function and the corresponding PV diagram are shown in Figure 25. Parabolic wider Ca2+ concentration function and the corresponding PV diagram are shown in Figure 26.

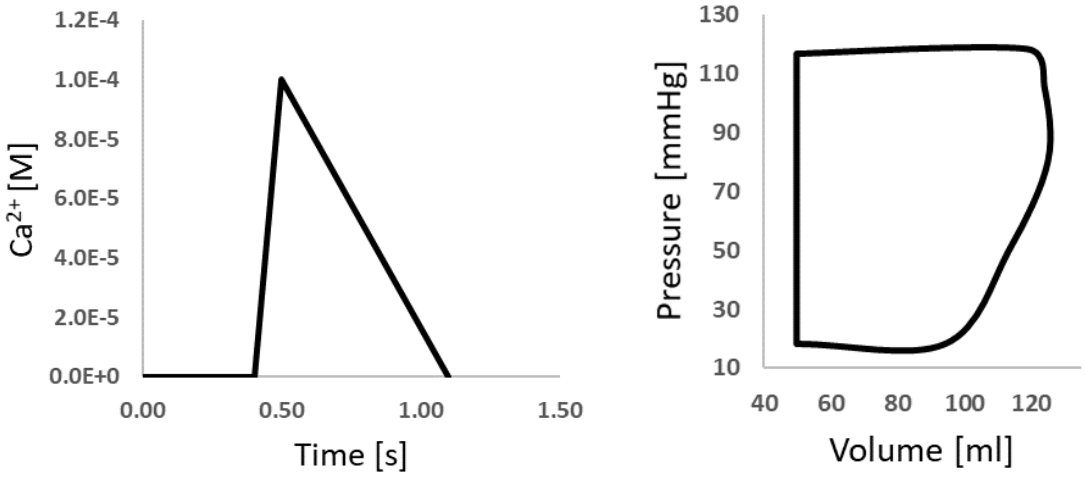

Figure 22. Triangular Ca^{2+} concentration and corresponding PV diagram

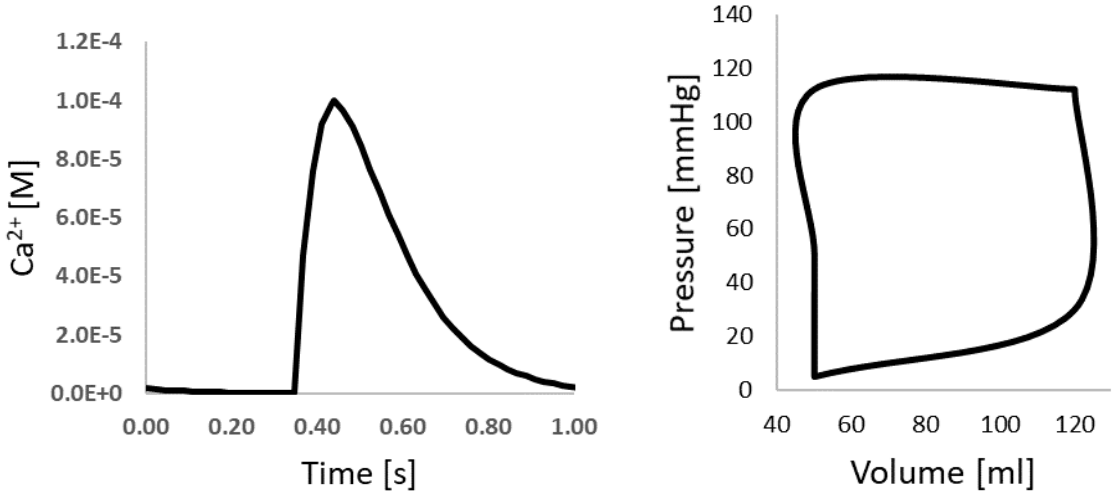

Figure 23. Parabolic Ca^{2+} concentration and corresponding PV diagram

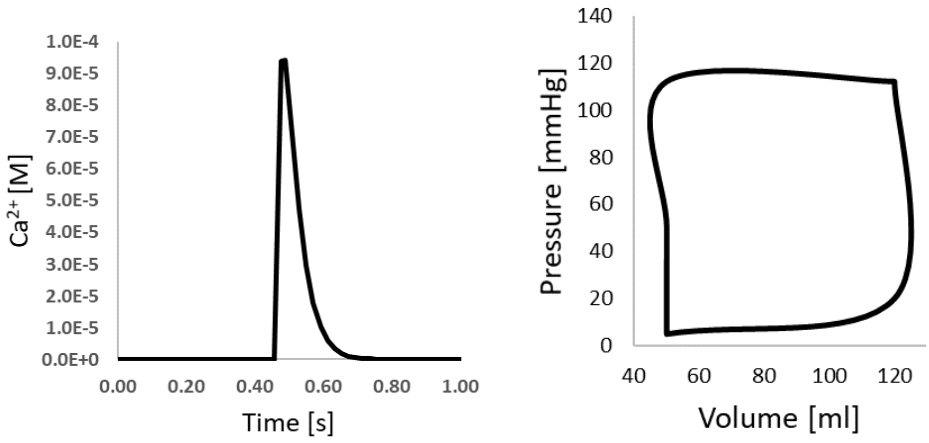

Figure 24. Steep Ca^{2+} concentration and corresponding PV diagram

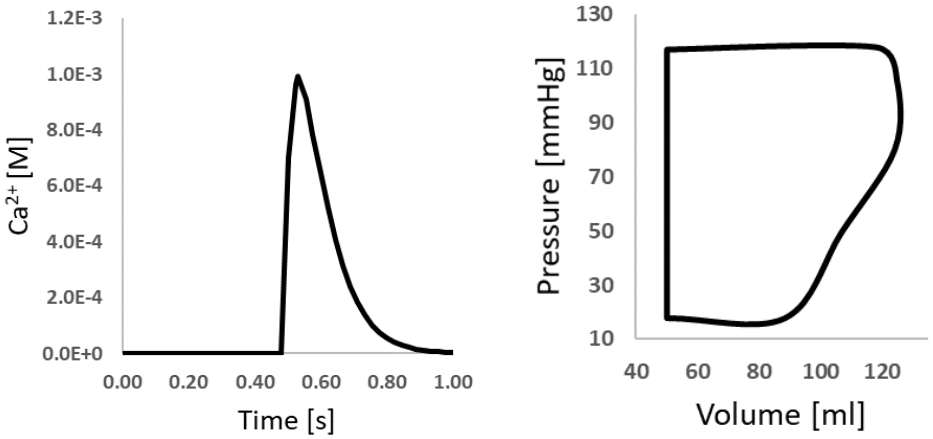

Figure 25. Shifted parabolic Ca2+ concentration and corresponding PV diagram

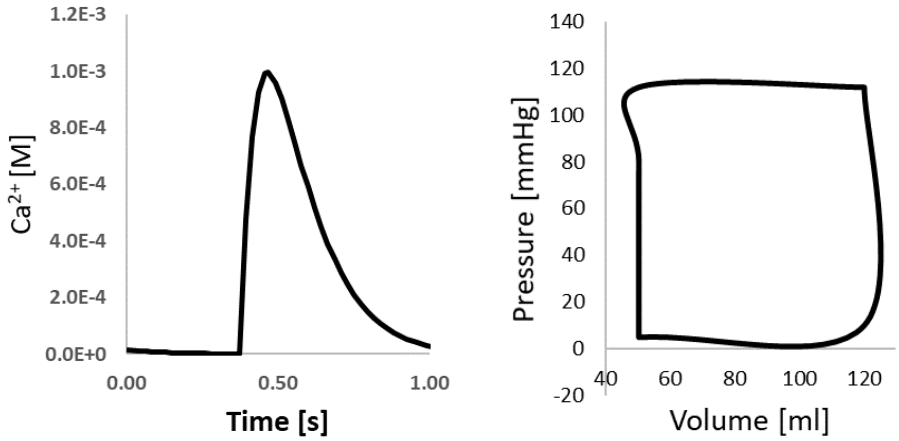

Figure 26. Parabolic wider Ca^{2+} concentration and corresponding PV diagram

This section includes result of PAK solver simulation with different LV geometry and corresponding scenarios. The first part (Section 3.1.5) is related to the results obtained from the LV model with 20% shorter base length. The second part (Section 3.1.6) is related to the results obtained from the LV model with 50% longer base length and 50% thicker lateral wall. Both cases cover three scenarios: i) Influence of Holzapfel scale factor (elasticity), ii) Influence of inlet and outlet velocities, and iii) Influence of Ca2+ concentration.

The presented approach with variation of LV geometry and simulations which include influence of different parameters on the PV diagrams are directly interlinked with drug effects on heart function.

This work is in continuous progress and it includes incorporation of different drugs that directly affect the cardiac PV diagrams and ejection fraction (e.g., angiotensin-converting enzyme inhibitors, angiotensin receptor blockers, nitrates, diuretics, calcium channel blockers).

3.1.5 Geometry of left ventricle with shorter base length

While in D8.1 the results of PAK solver tool are presented for full base length of heart, in this chapter, we will show results obtained from our left ventricle model with 20% shorter base length. Geometry of this model is shown in Figure 27.

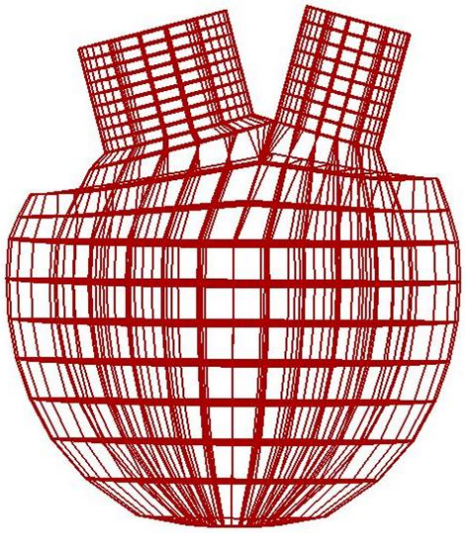

Figure 27. Geometry of left ventricle model with 20% shorter base

3.1.5.1 Scenario 3b: Influence of Ca^{2+} concentration

Triangular Ca^{2+} concentration function is shown in Figure 28 along with corresponding PV diagram. Parabolic Ca2+ concentration function and corresponding PV diagram are shown in Figure 29. Steep Ca2+ concentration function and corresponding PV diagram are shown in Figure 30. Shifted parabolic Ca2+ concentration function and corresponding PV diagram are shown in Figure 31. Parabolic wider Ca2+ concentration function and corresponding PV diagram are shown in Figure 32.

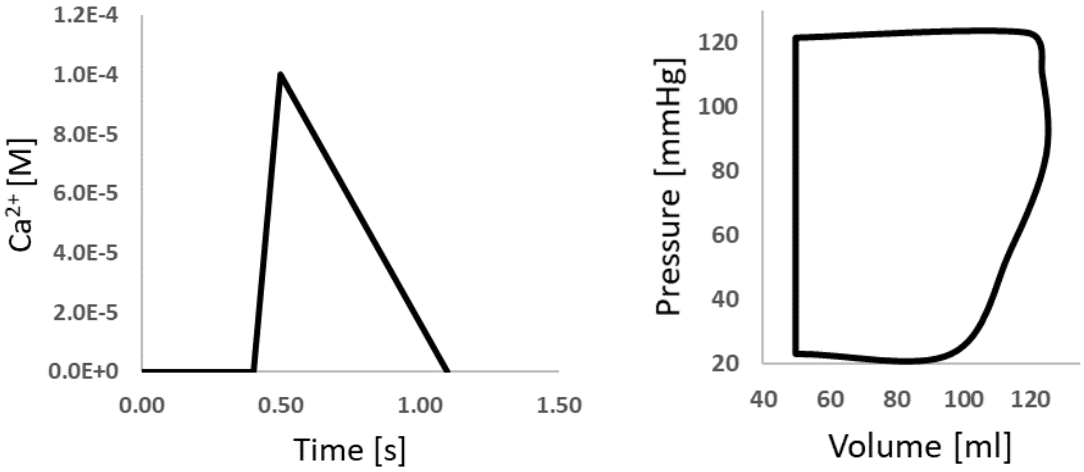

Figure 28. Triangular Ca^{2+} concentration and corresponding PV diagram

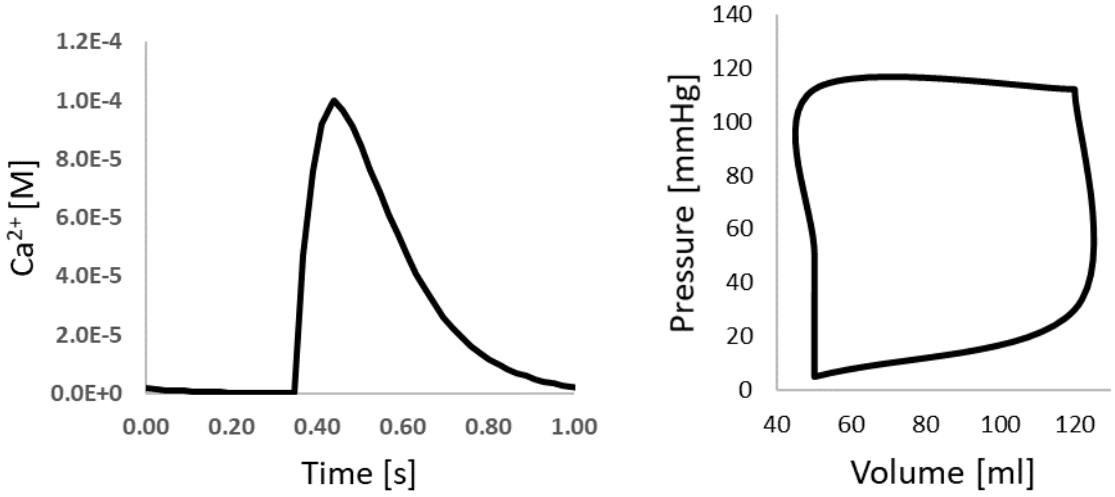

Figure 29. Parabolic Ca^{2+} concentration and corresponding PV diagram

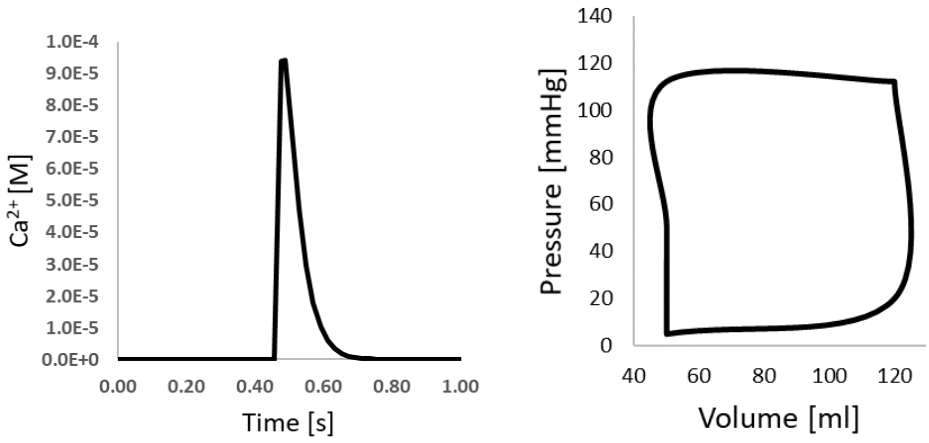

Figure 30. Steep Ca^{2+} concentration and corresponding PV diagram

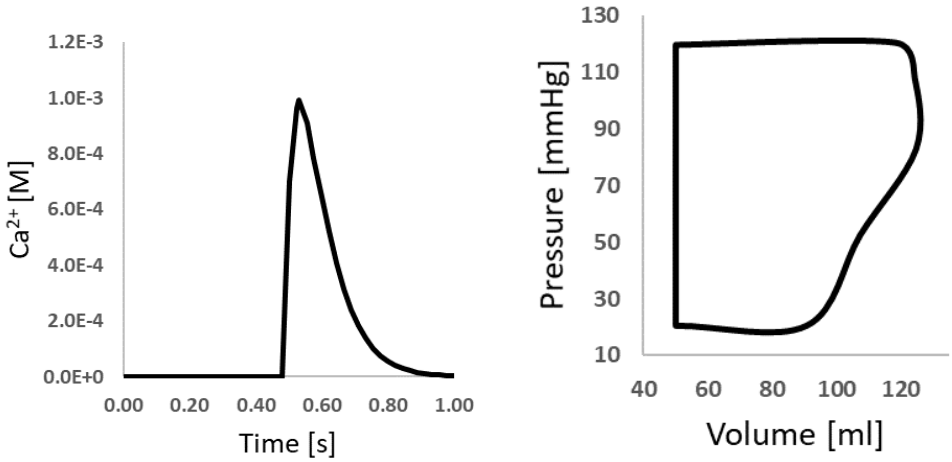

Figure 31. Shifted parabolic Ca+ concentration and corresponding PV diagram

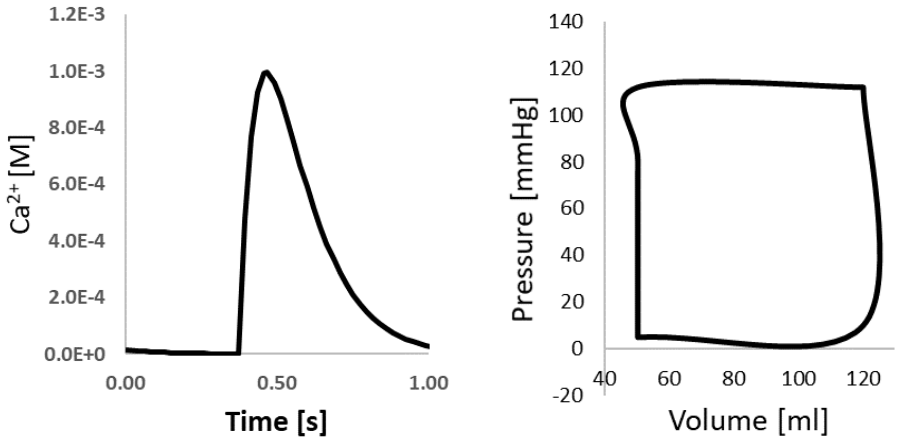

Figure 32. Parabolic wider Ca^{2+} concentration and corresponding PV diagram

Displacement field at 0.2s, 0.5s and 0.6s is shown in Figure 33. Velocity field at 0.2s, 0.5s and 0.6s is shown in Figure 34. Pressure field at 0.2s, 0.5s and 0.6s is shown in Figure 35.

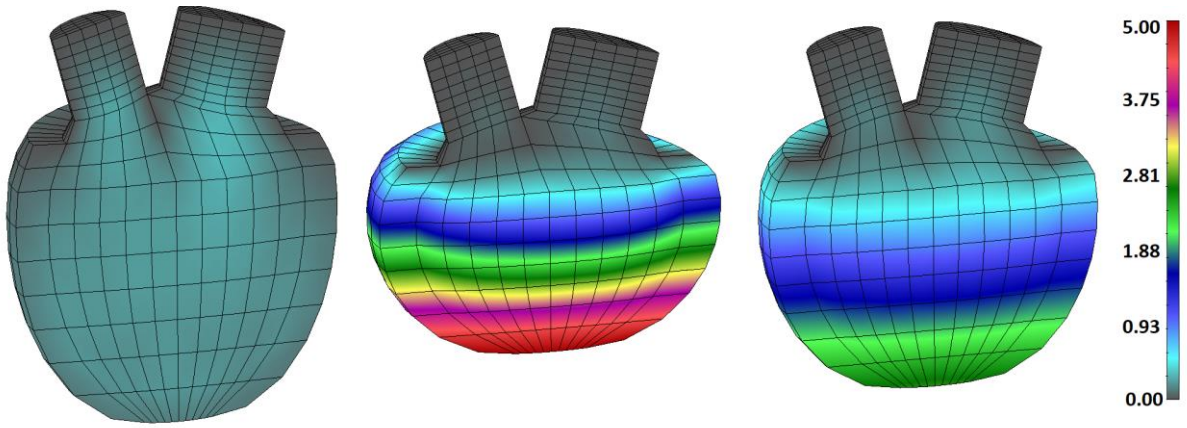

Figure 33. Displacement field at 0.2s, 0.5s and 0.6s for parabolic Ca^{2+} concentration function

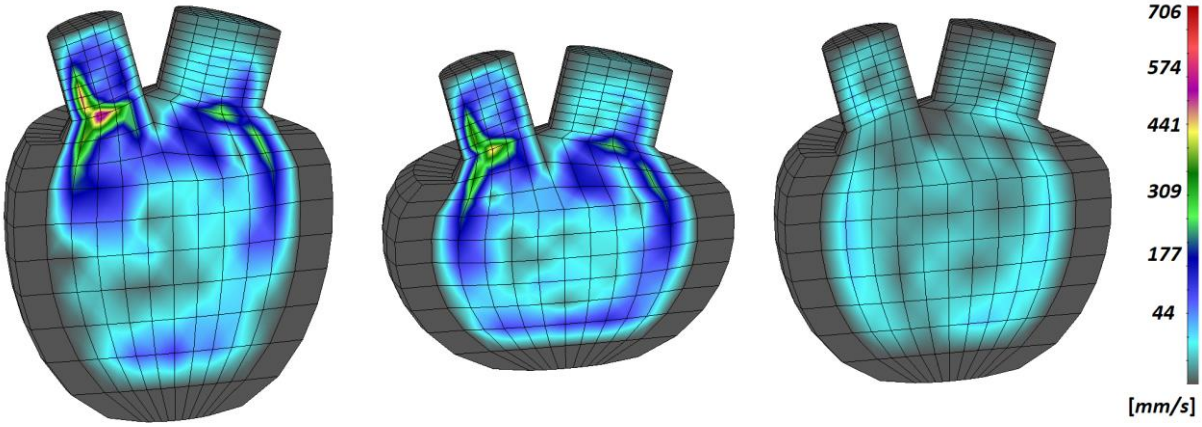

Figure 34. Velocity field at 0.2s, 0.5s and 0.6s for parabolic Ca^{2+} concentration function

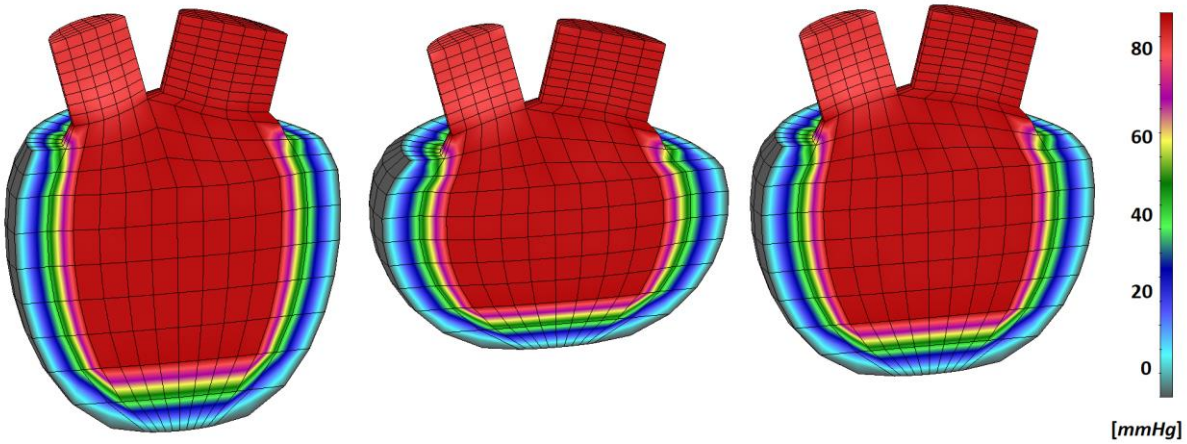

Figure 35. Pressure field at 0.2s, 0.5s and 0.6s for parabolic Ca^{2+} concentration function

Effect of different Ca2+ concentration functions to the ejection fraction is shown in Figure 36.

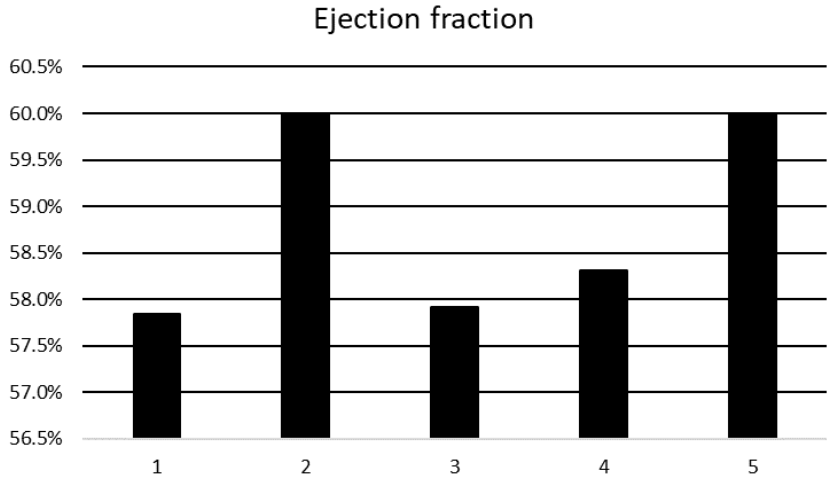

Figure 36. Ejection fraction for (1) triangular, (2) parabolic, (3) steep, (4) shifted parabolic and (5) parabolic wider Ca2+ concentration function

3.1.5.2 Scenario 1b: Influence of Holzapfel scale factor (elasticity)

In this section, we will examine the influence of elasticity to cardiac cycle. PV diagrams for 20% higher and 20% lower elasticity are shown in Figure 37. PV diagrams for 30% higher and 50% lower elasticity are shown in Figure 38. Effect of the elasticity to the ejection fraction is shown in Figure 39.

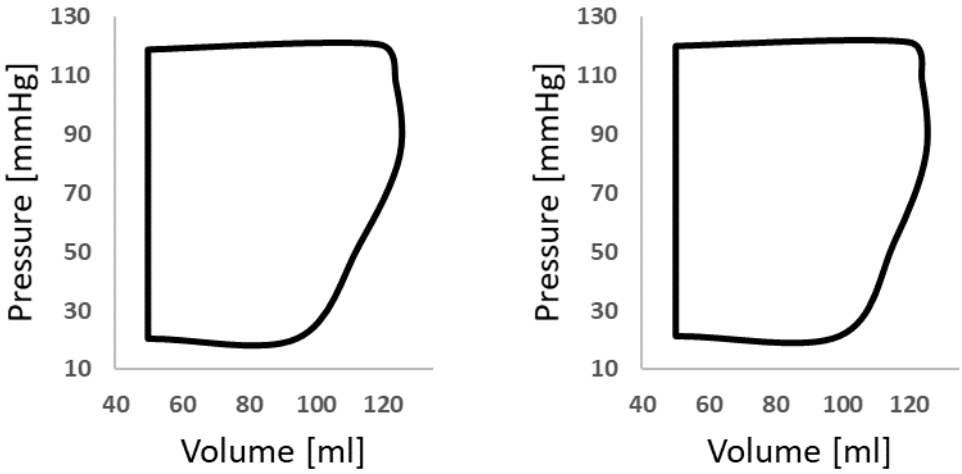

Figure 37. PV diagrams for 20 % higher (left) and 20% lower (right) elasticity

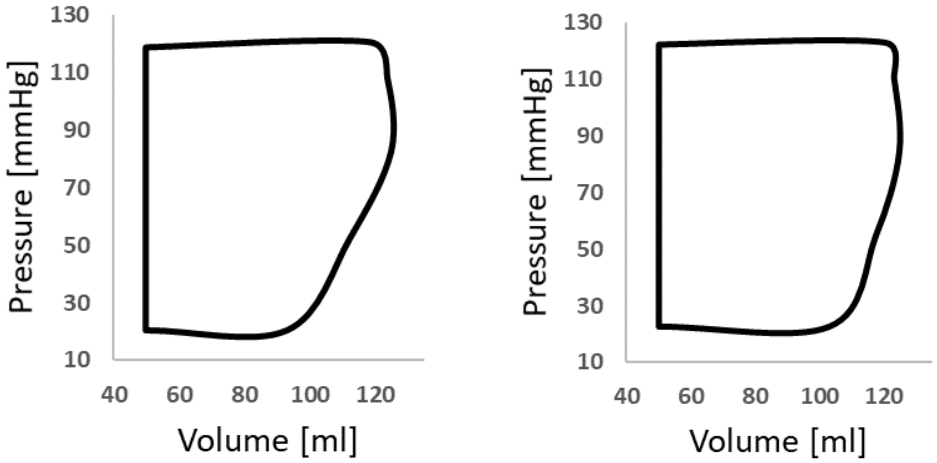

Figure 38. PV diagrams for 30 % higher (left) and 50% lower (right) elasticity

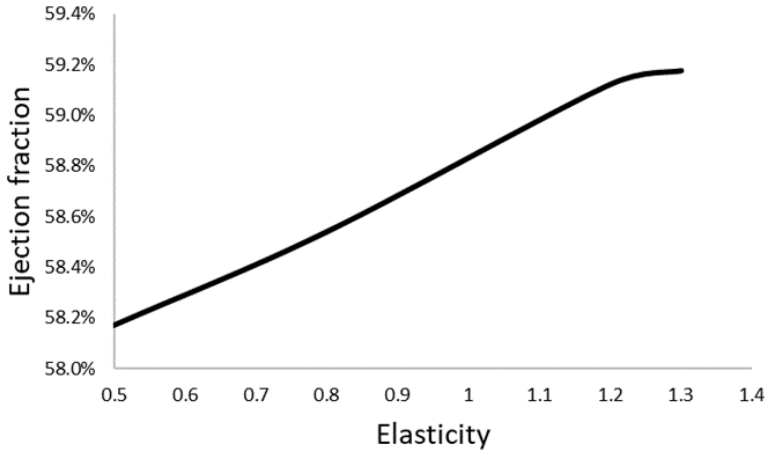

Figure 39. Effect of the elasticity to the ejection fraction

3.1.5.3 Scenario 2b: Influence of inlet and outlet velocities

PV diagrams for 25% higher inlet velocities and 25% higher outlet velocities are shown in Figure 40. V diagrams for 25% lower inlet velocity and 25% lower outlet velocity are shown in Figure 41. In Figure 42, we have shown the effect of inlet velocity to ejection fraction. In Figure 43, we have shown the effect of outlet velocity to ejection fraction.

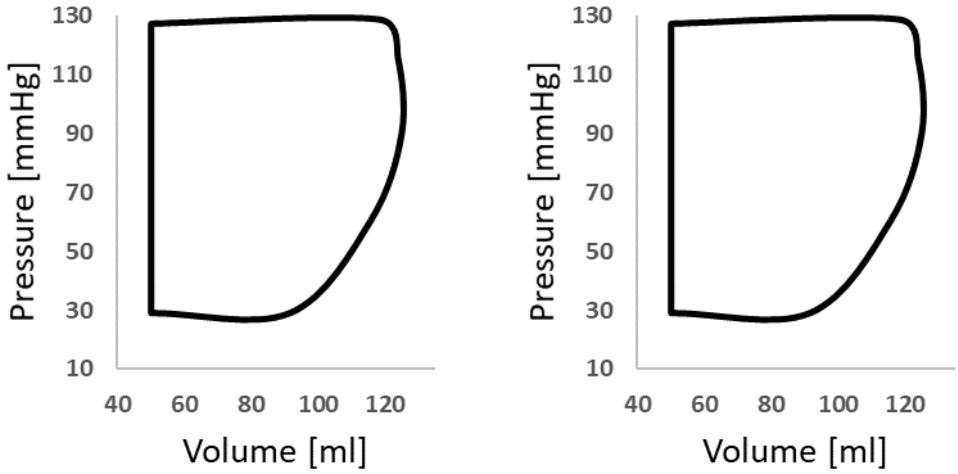

Figure 40. PV diagrams for Inlet velocity from the left atrium 25% higher (left) and outlet velocity 25% higher (right)

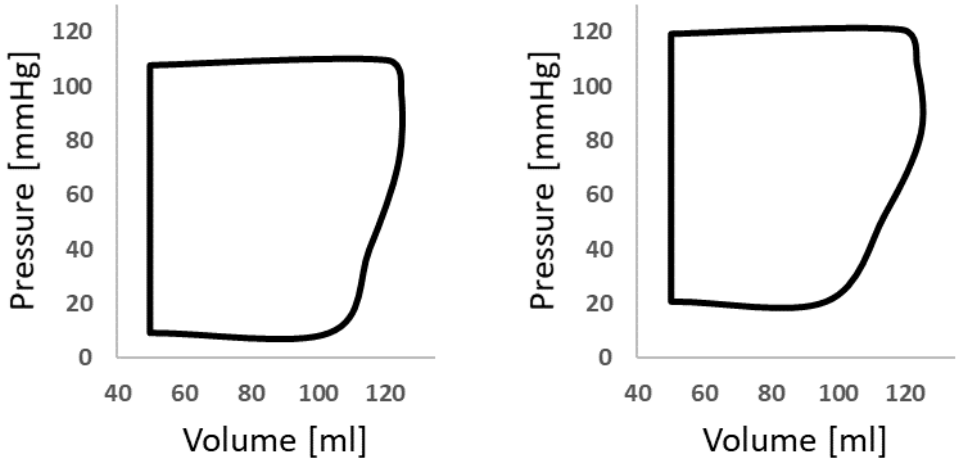

Figure 41. PV diagrams for Inlet velocity from the left atrium 25% lower (left) and outlet velocity 25% lower (right)

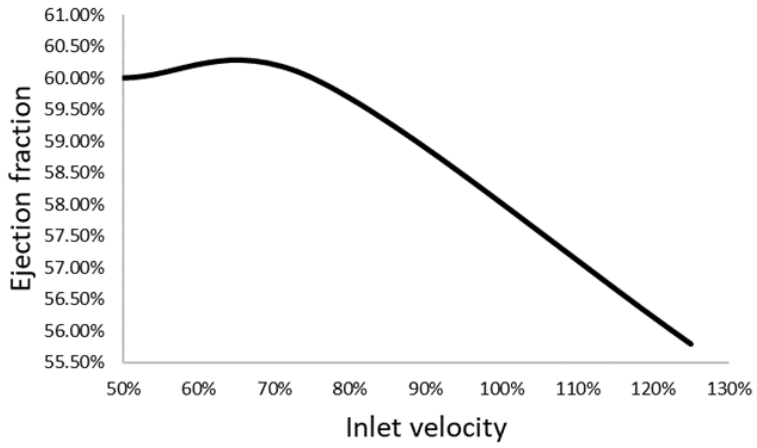

Figure 42. Ejection fraction with respect to inlet velocity

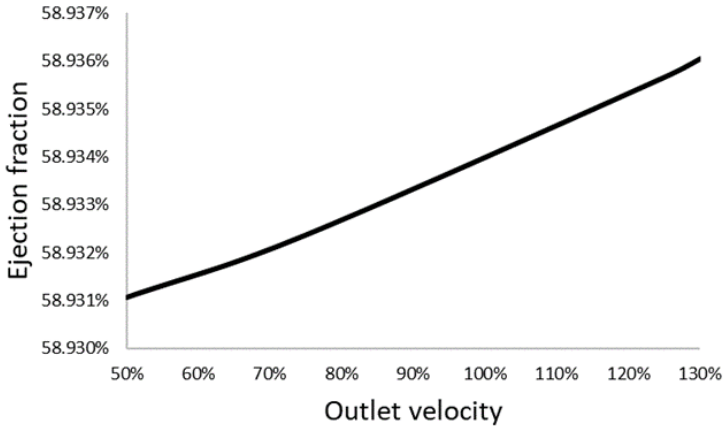

Figure 43. Ejection fraction with respect to outlet velocity

3.1.6 Geometry of left ventricle with longer base length and thicker lateral wall

Different drugs have different pathways which directly affect the functional heart working. Detailed description of mechanism for basic groups of the drugs like Angiotensin-converting enzyme (ACE) inhibitors, Angiotensin receptor blockers (ARBs), Nitric oxide-induced vasodilators, Diuretics, Calcium Channel Blockers have been included in Section 6.2 in D8.1. These drugs have a direct influence on the cardiac PV diagrams and ejection fraction.

In this chapter, we will show results obtained from our left ventricle model with 50% longer base length and 50% thicker lateral wall. Geometry is shown in Figure 44.

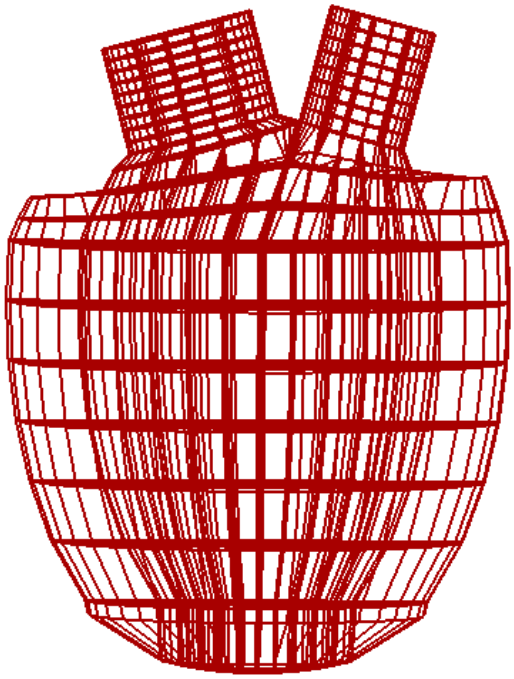

Figure 44. Geometry of left ventricle model with 50% longer base and 50% thicker lateral wall

3.1.6.1 Scenario 3c: Influence of Ca^{2+} concentration

Triangular Ca^{2+} concentration function is shown in Figure 45 along with corresponding PV diagram. Parabolic Ca2+ concentration function and corresponding PV diagram are shown in Figure 46. Steep Ca2+ concentration function and corresponding PV diagram are shown in Figure 47. Shifted parabolic Ca2+ concentration function and corresponding PV diagram are shown in Figure 48. Parabolic wider Ca2+ concentration function and corresponding PV diagram are shown in Figure 49.

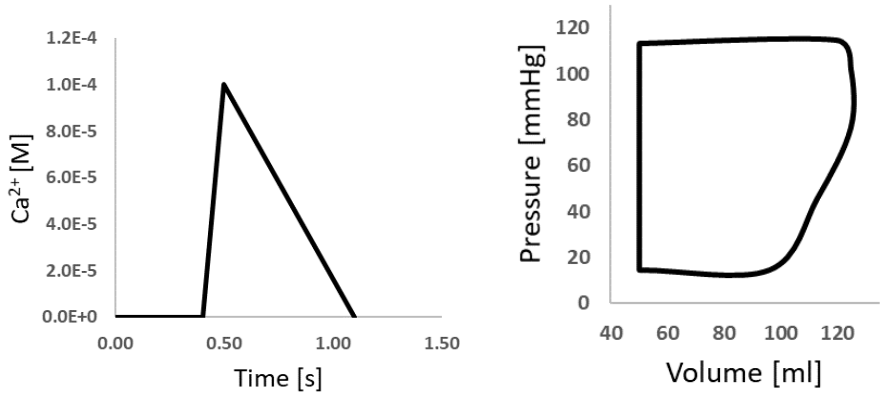

Figure 45. Triangular Ca^{2+} concentration and corresponding PV diagram

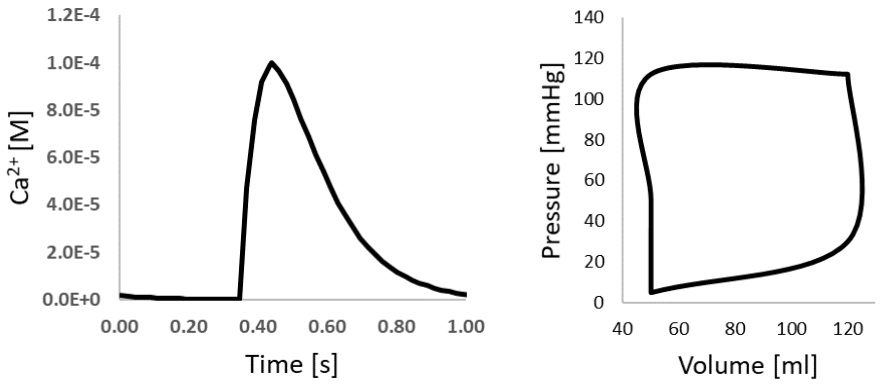

Figure 46. Parabolic Ca^{2+} concentration and corresponding PV diagram

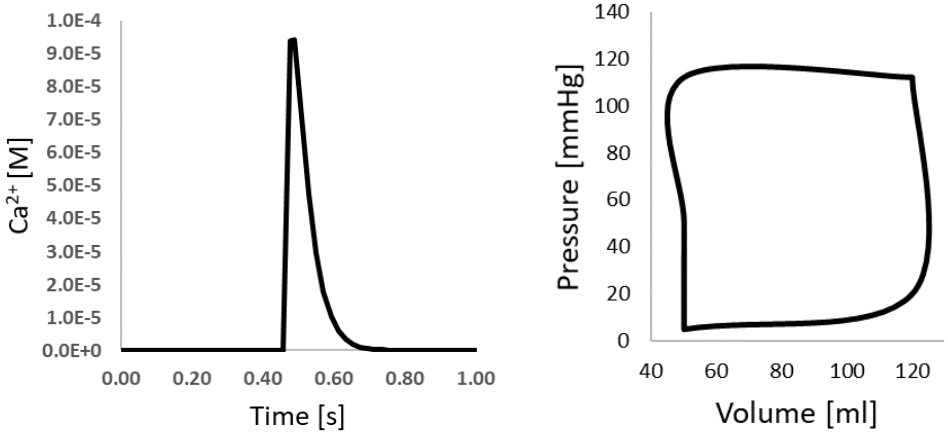

Figure 47. Steep Ca^{2+} concentration and corresponding PV diagram

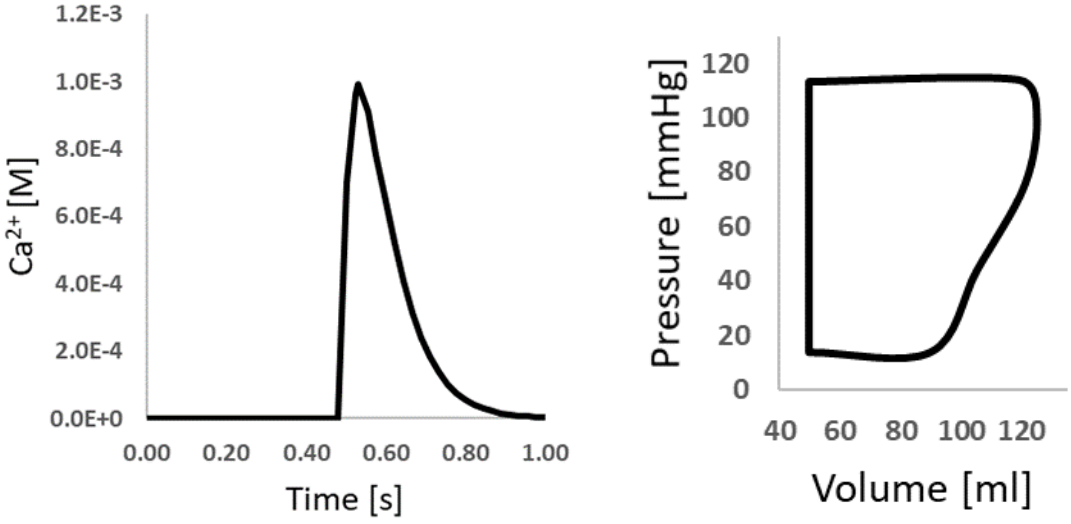

Figure 48. Shifted parabolic Ca^{2+} concentration and corresponding PV diagram

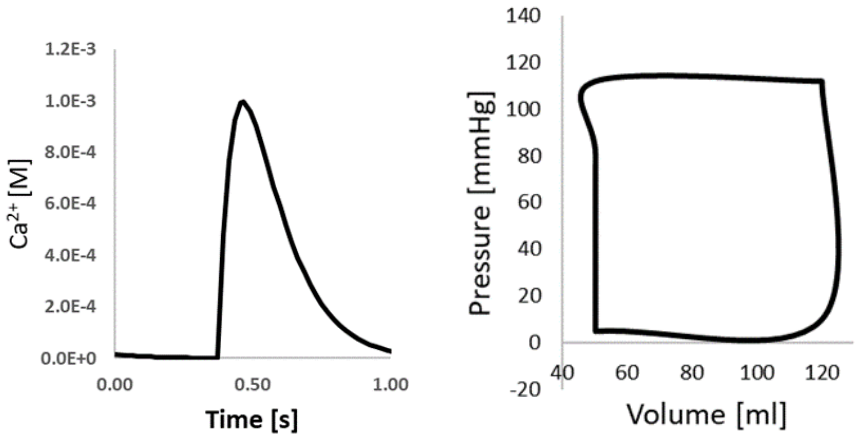

Figure 49. Parabolic wider Ca^{2+} concentration and corresponding PV diagram

Displacement field at 0.2s, 0.5s and 0.6s is shown in Figure 50. Velocity field at 0.2s, 0.5s and 0.6s is shown in Figure 51. Pressure field at 0.2s, 0.5s and 0.6s is shown in Figure 52. Effect of different Ca2+ concentration functions to the ejection fraction is shown in Figure 53.

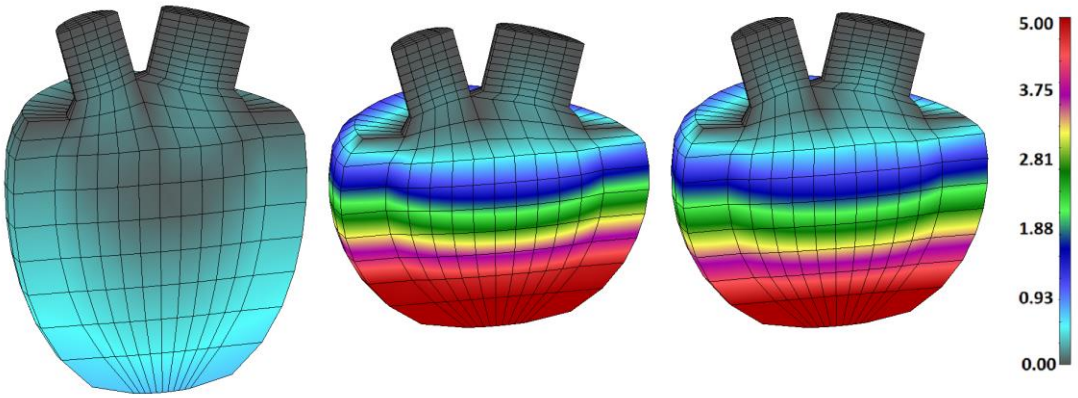

Figure 50. Displacement field at 0.2s, 0.5s and 0.6s with parabolic Ca^{2+} concentration function

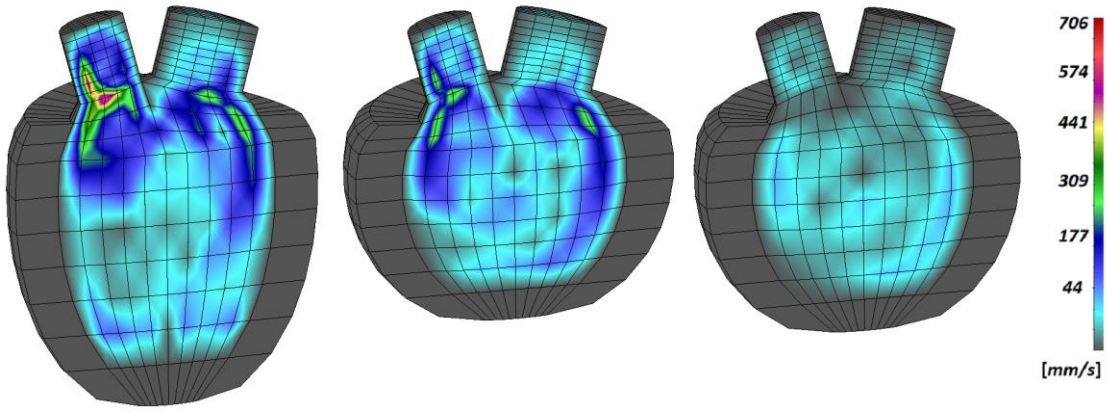

Figure 51. Velocity field at 0.2s, 0.5s and 0.6s with parabolic Ca^{2+} concentration function

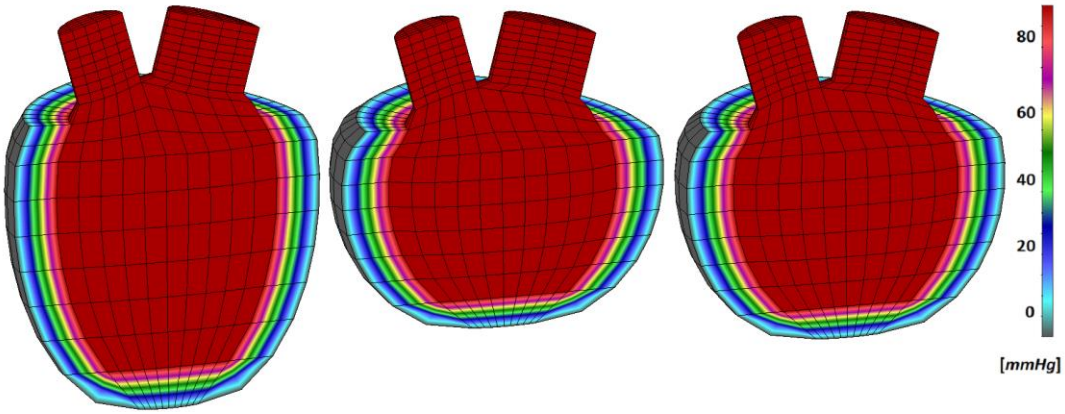

Figure 52. Pressure field at 0.2s, 0.5s and 0.6s with parabolic Ca^{2+} concentration function

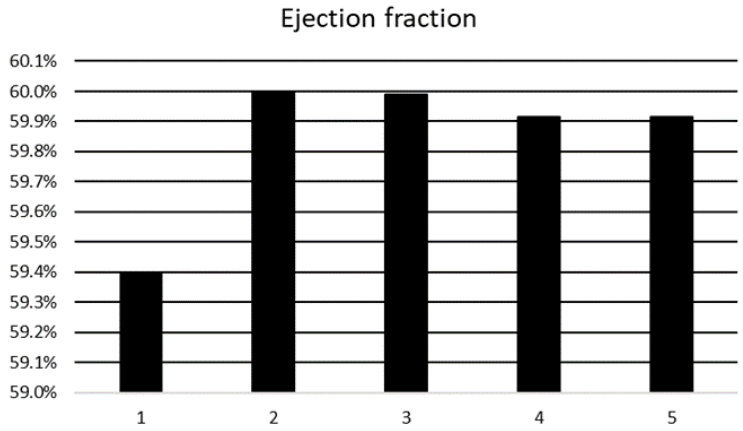

Figure 53. Ejection fraction for (1) triangular, (2) parabolic, (3) steep, (4) shifted parabolic and (5) parabolic wider Ca2+ concentration function

3.1.6.2 Scenario 1c: Influence of Holzapfel scale factor (elasticity)

In this section, we will examine the influence of elasticity to cardiac cycle. PV diagrams for 20% higher and 20% lower elasticity are shown in Figure 54. PV diagrams for 30% higher and 50% lower elasticity are shown in Figure 55. Effect of the elasticity to the ejection fraction is shown in Figure 56.

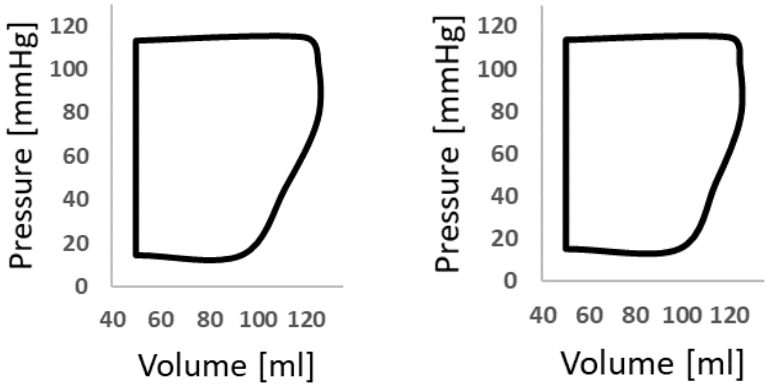

Figure 54. PV diagrams for 20 % higher (left) and 20% lower (right) elasticity

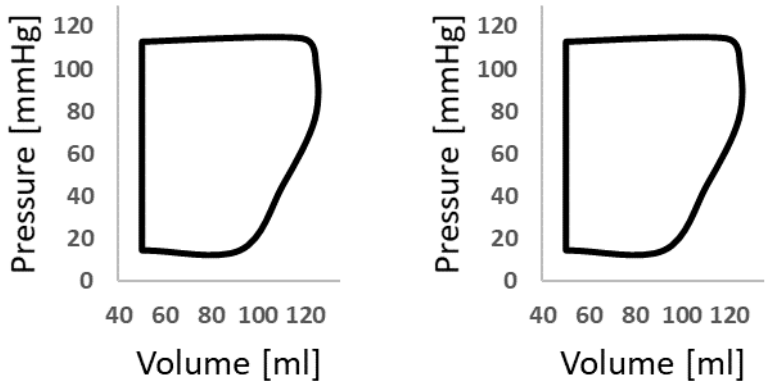

Figure 55. PV diagrams for 30 % higher (left) and 50% lower (right) elasticity

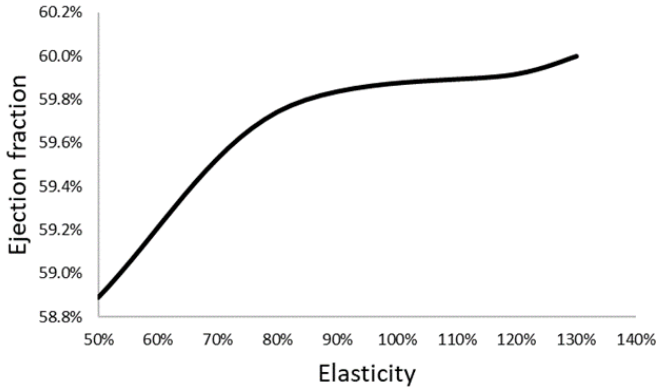

Figure 56. Effect of the elasticity to the ejection fraction

3.1.6.3 Scenario 2c: Influence of inlet and outlet velocities

PV diagrams for 50% lower inlet velocity and 50% lower outlet velocity are shown in Figure 57. PV diagrams for 30% higher inlet velocity and 30% higher outlet velocity are shown in Figure 58. In Figure 59, we presented the effect of inlet velocity to ejection fraction. In Figure 60, we showed the effect of outlet velocity to ejection fraction.

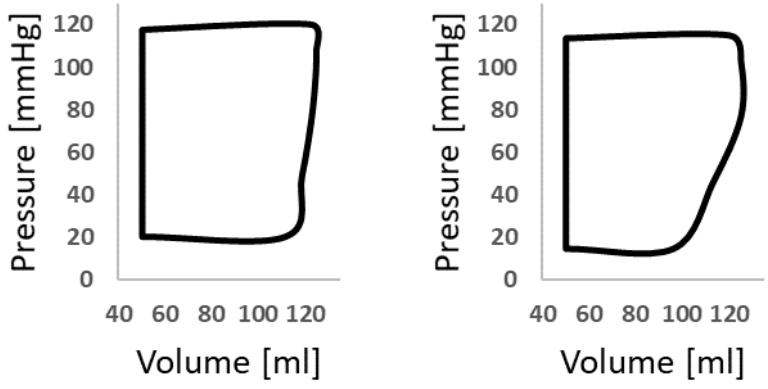

Figure 57. PV diagrams for Inlet velocity from the left atrium 50% lower (left) and outlet velocity 50% lower (right)

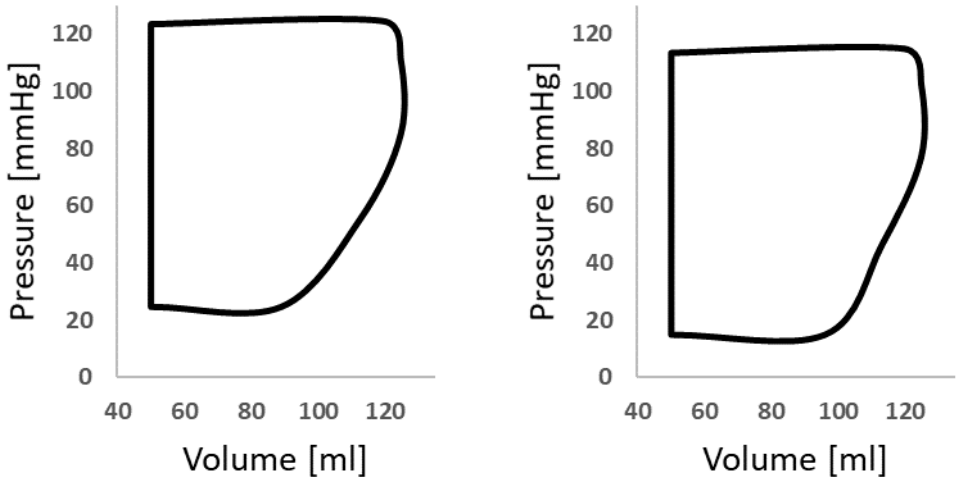

Figure 58. PV diagrams for Inlet velocity from the left atrium 30% higher (left) and outlet velocity 30% higher (right)

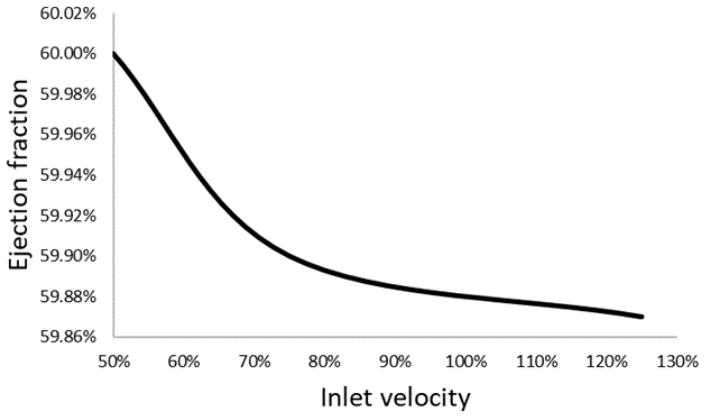

Figure 59. Ejection fraction with respect to inlet velocity

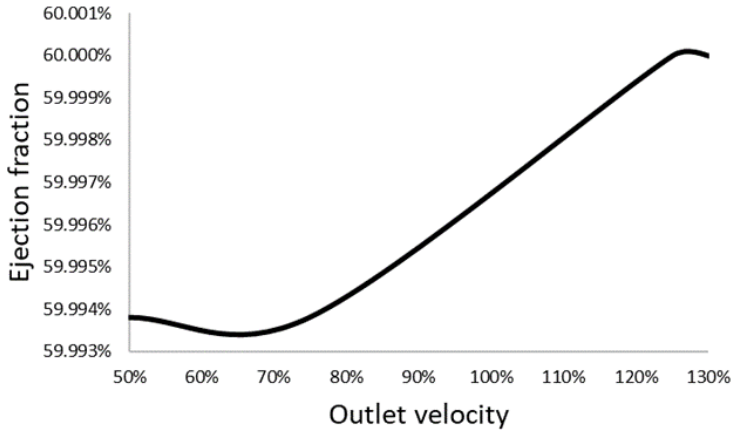

Figure 60. Ejection fraction with respect to outlet velocity

3.2 Drug influence on the ECG simulation and comparison with ECG clinical measurement

Cardiac cells are filled with and surrounded by an ionic solution, mostly sodium *Na*+, potassium *K*+, and calcium *Ca*2+. These charged atoms move between the inside and the outside of the cell through proteins called ion channels. Cells are connected through gap junctions, which form channels that allow ions to flow from one cell to another.

An accurate numerical model is needed for better understanding of heart behaviour in cardiomyopathy, heart failure, cardiac arrhythmia, and other heart diseases. These numerical models usually include drug transport, electrophysiology and muscle mechanics. We have presented heart geometry and seven different regions of the model where we included: 1) Sinoatrial node; 2) Atria; 3) Atrioventricular node; 4) His bundle; 5) Bundle fibres; 6) Purkinje fibres; 7) Ventricular myocardium (Figure 61).

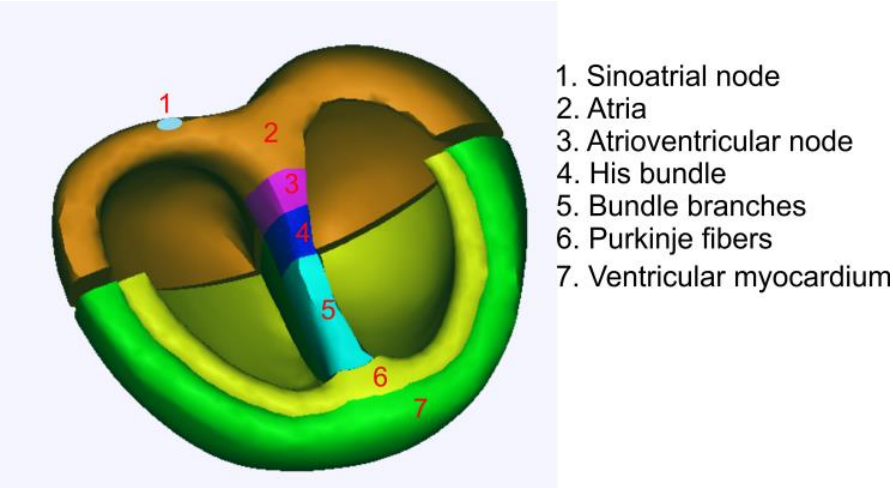

Figure 61. Heart geometry and seven different regions of the model

Parameters for the regions presented in the figure above are given in Table 20.

Table 20. Parameters for the monodomain model with modified FitzHugh-Nahumo equations

Parameter	SAN	Atria	AVN	His	BNL	Purkinje	Ventricles
a	-0.60	0.13	0.13	0.13	0.13	0.13	0.13
b	-0.30	0	0	0	0	0	0
c_1(AsV^{-1} m^{-3})	1000	2.6	2.6	2.6	2.6	2.6	2.6
c_2 (AsV^{-1} m^{-3})	1.0	1.0	1.0	1.0	1.0	1.0	1.0
D	0	1	1	1	1	1	1
e	0.066	0.0132	0.0132	0.005	0.0022	0.0047	0.006
A (mV)	33	140	140	140	140	140	140
B (mV)	-22	-85	-85	-85	-85	-85	-85
k	1000	1000	1000	1000	1000	1000	1000
σ ($mS \cdot m^{-1}$)	0.5	8	0.5	10	15	35	8

The whole heart activation simulation from lead II ECG signal at various time points on the ECG signal for patient #1 and #2 have been presented in Figure 62. and Figure 64. Comparison of the simulated

ECG on the surface body with real ECG measurement at V1 for patients #1 and #2 have been presented in Figure 63 and Figure 65.

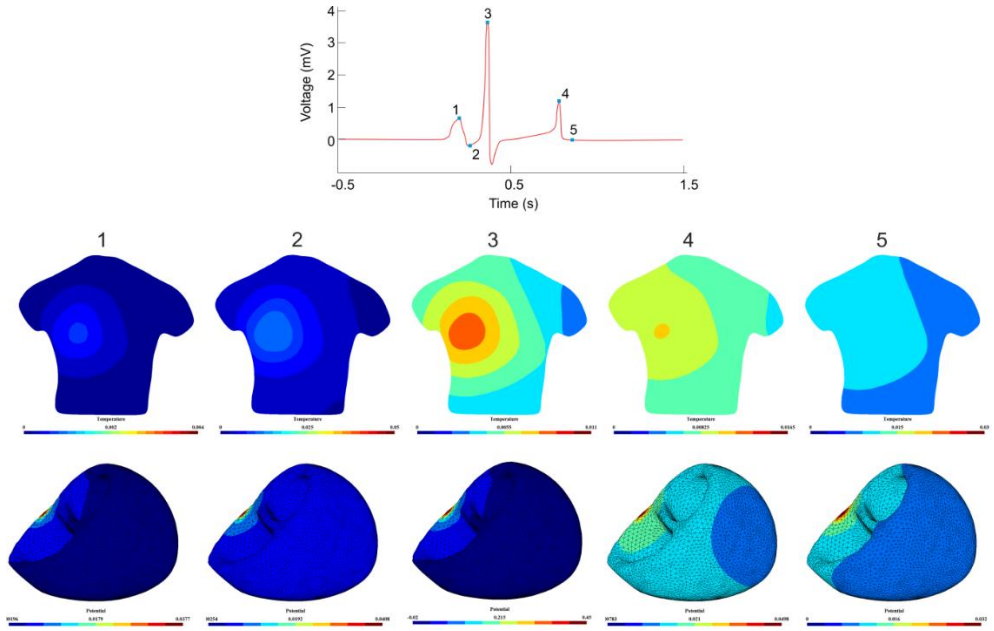

Figure 62. Patient #1: whole heart activation simulation from lead II ECG signal at various time points on the ECG signal. There are 1-5 activation sequences corresponding to ECG signal above. The colour bar denotes mV of the transmembrane potential.

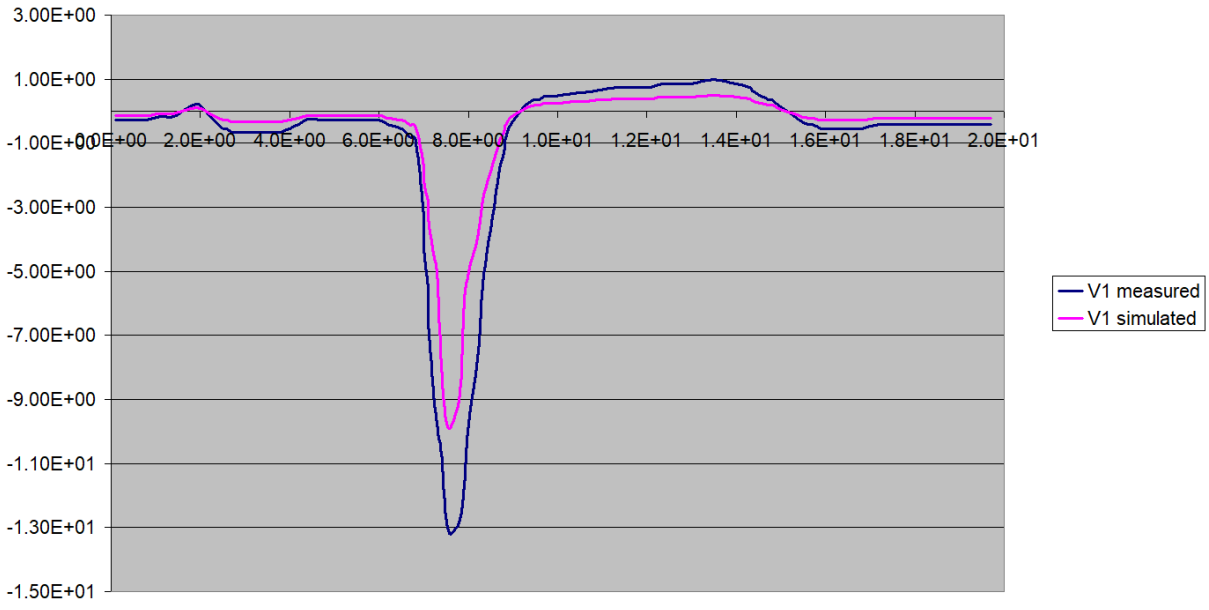

Figure 63. Patient #1: Comparison of the simulated ECG on the surface body with real ECG measurement at V1

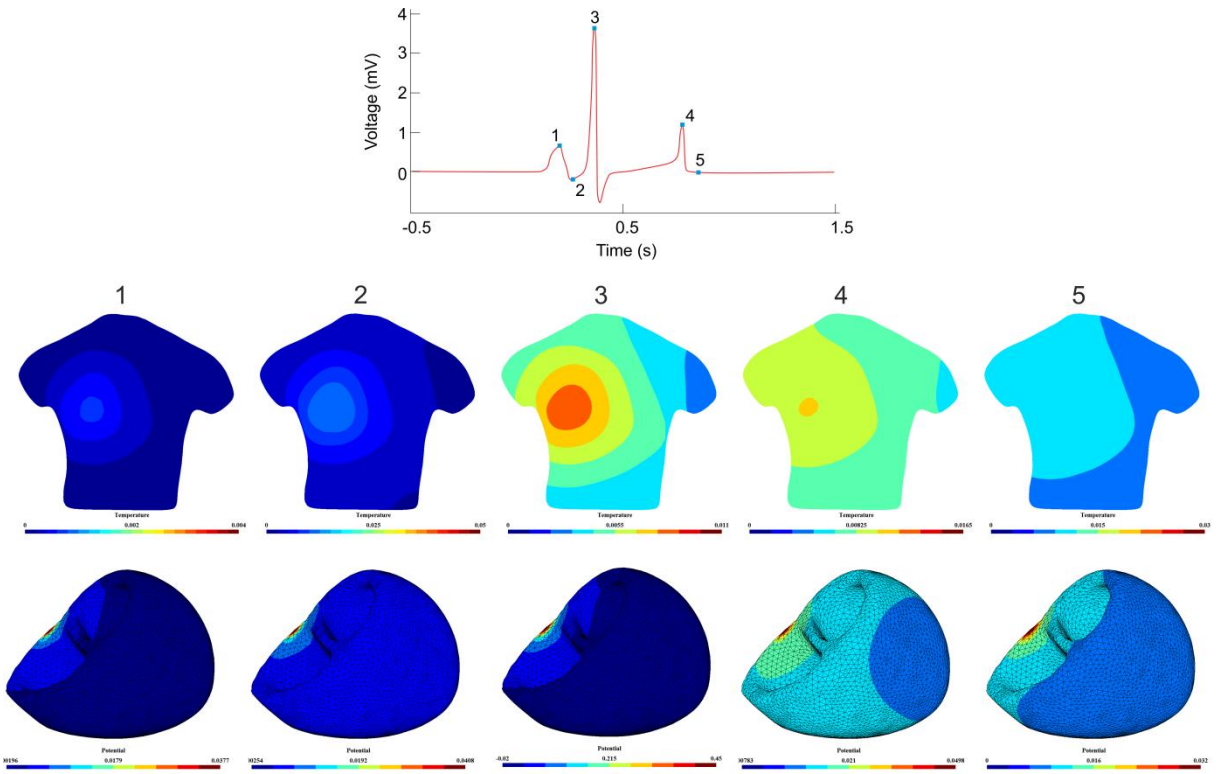

Figure 64. Patient #2: whole heart activation simulation from lead II ECG signal at various time points on the ECG signal. There are 1-5 activation sequences corresponding to ECG signal above. The color bar denotes mV of the transmembrane potential.

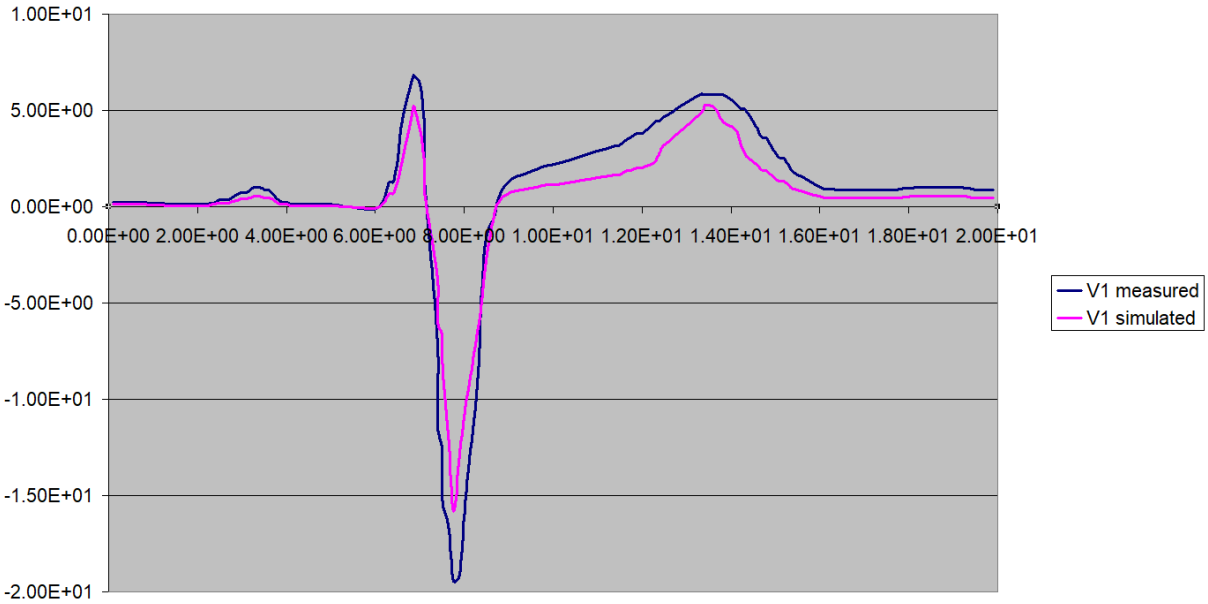

Figure 65. Patient #2: Comparison of the simulated ECG on the surface body with real ECG measurement at V1

3.2.1 Realistic geometry of heart model with left chamber and atrium parts surrounded by solid wall and standard inlet and outlet velocity profiles

Using experimental data and DICOM files provided, we have reconstructed realistic heart model as STL format with left atrium (Figure 66a, noted blue) and chamber part (Figure 66a, noted yellow) with accompanying mitral valve cross-section between (Figure 66a, noted green), and also aortic part (Figure 66a, noted orange) of the model with aortic cross-section included in fluid part of the model, which is surrounded by solid wall (Figure 66a, wireframe). Finite element model consists of 139896 hexahedral 3D elements, divided by 161989 nodes. Model geometry is generated using STL files. Solid nodes are constrained around inlet/ outlet cross-sections (Figure 66a; red and magenta rings), and in the zone close to the mitral valve cross-section. Other solid nodes are free. On Figure 66c, 2 cross-section regions are marked to define prescribed inlet and outlet zones. Inside the fluid domain, we have mitral valve cross-section (part of the model between ventricle and atrium; Figure 66c, red line) with inlet velocity function profile prescribed (Figure 66a), and aortic valve cross-section (part between ventricle and aortic branch, Figure 66c, green line), with outlet velocity function profile prescribed (Figure 66b). Fibers direction in solid domain of realistic heart model are showed in Figure 66b, and section C on the same figure shows distribution of velocity field in realistic heart model, at 0.1s. It can be seen that velocity values are the highest at inlet and outlet boundary cross-sections (red and green lines, Figure 66c), which is logical due to prescribed inlet function and prescribed values at that cross-section at the beginning of simulation. Regarding the material models used, we have selected Holzapfel material model for obtaining passive stresses in the heart wall, and for muscle activation we used Hunter material model for active stresses. Activation of the muscle is achieved using calcium function, displayed in Figure 67c.

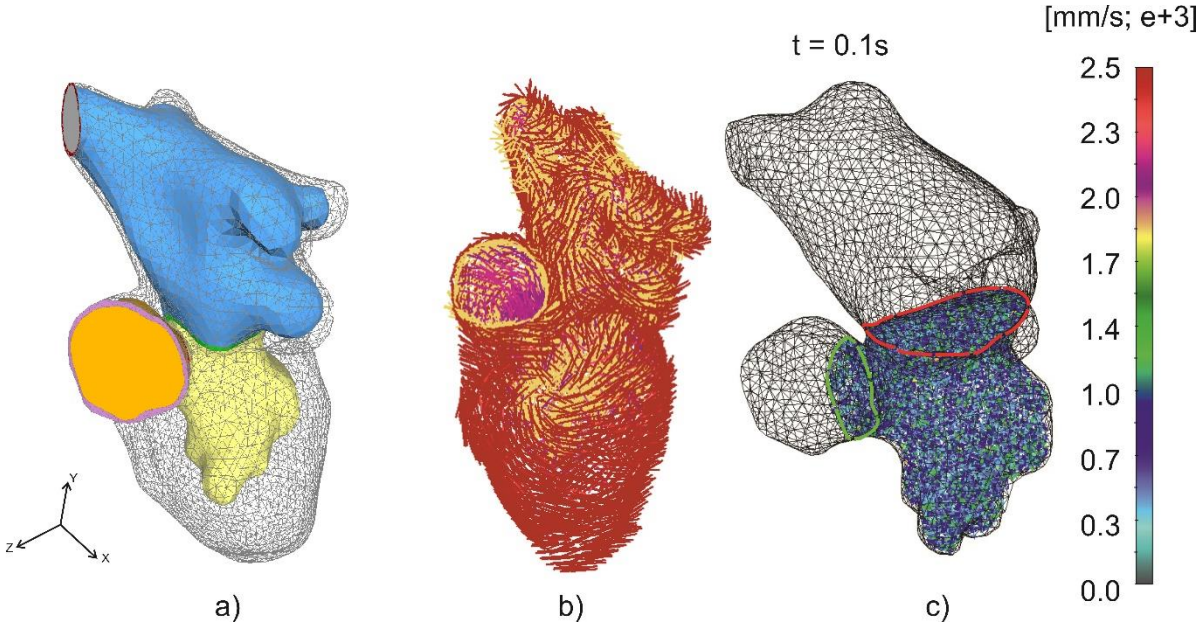

Figure 66. a) Realistic heart FE model with representative cross- sections and fluid parts; b) Direction of fibres in solid part of realistic model; c) Fluid velocity field at 0.1s (mitral and aortic cross-section noted).

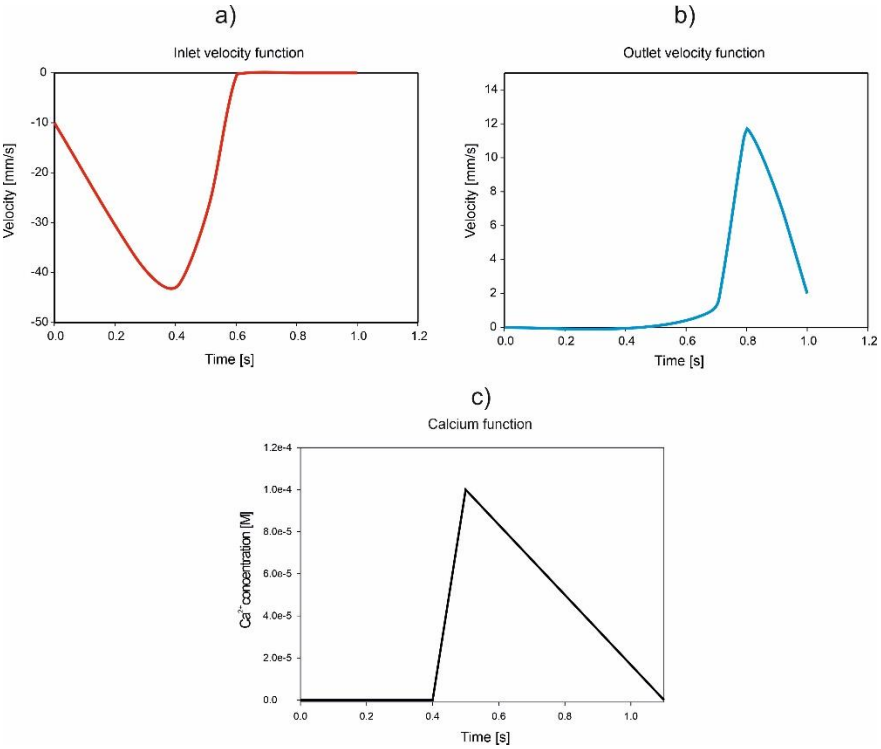

Figure 67. a) Inlet function of velocity, at mitral valve cross-section; b) outlet velocity function – at aortic valve cross-section; c) Calcium concentration function used for activation of the muscle.

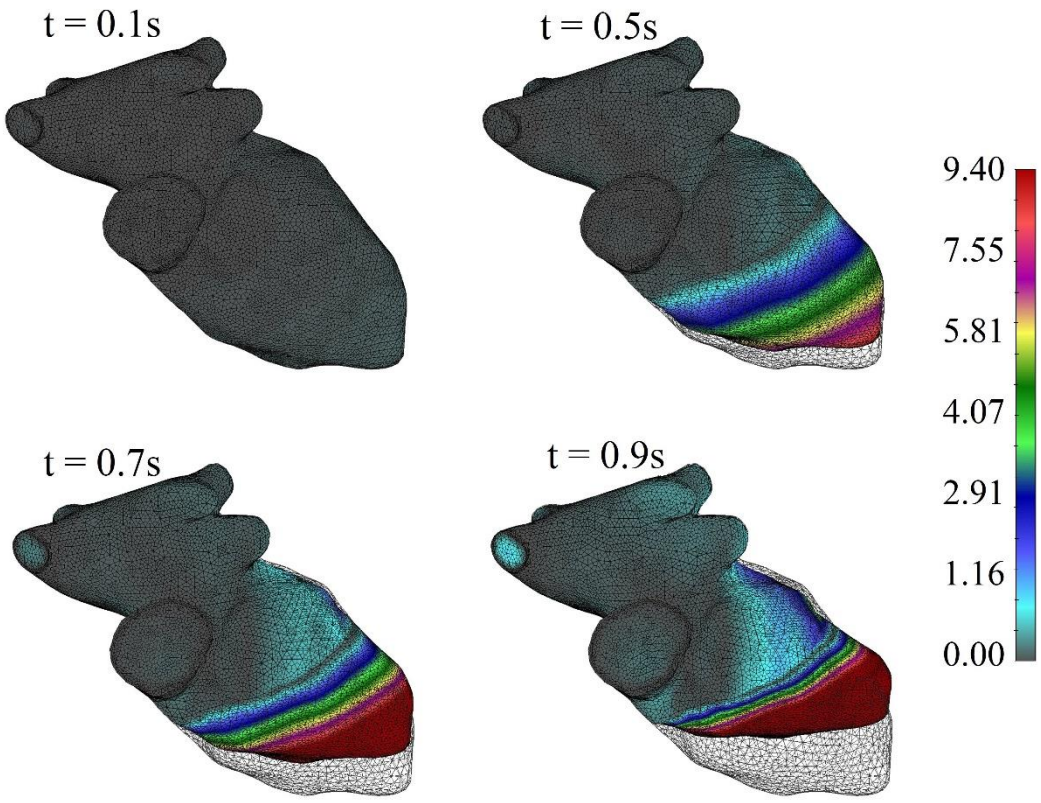

Figure 68. Field of displacements in solid wall of realistic model of heart; four different time periods. Non-deformed configuration noted as black mesh part.

Field of displacements in solid wall of realistic model of heart, during 4 different time steps of one cardiac cycle, is given in Figure 68. At first step (0.1s), just the passive part of the material model has an impact on solid wall structure and until 0.4s of simulation model volume is increasing until the mitral cross-section is opened and fluid flows into the left chamber part. When the mitral valve is closed and injection of fluid is finished, fluid starts to eject from the chamber through the aortic cross-section, calcium function inside Hunter material model starts to act (0.5s), causing the start of the muscle contraction until the 0.9s of simulation after which model slowly returns to its undeformed state.

4. Deviation from the work plan

The presented document is revised and updated version of the D8.1 submitted on June 7th 2021. After the project review meeting which was held on July 5th 2021, the review team rejected the deliverable and gave the recommendations how it should be improved. The agreed deadline was end of October 2021. Consortium took all comments and recommendations from the review team into consideration and submitted the updated deliverable on 02/11/2021.

5. Conclusions

The revised deliverable D8.2 “Computational pipelines for drug testing” corresponds to the work performed within Task 8.2 “2 Set up R&D computation pipelines for drug testing” (M24-M36) of the SILICOFCM project. The performed work is related to WP4, WP5 and WP6, and should be read together with D8.1 “Workflow for drug testing”. In addition, the document is interlinked with D8.3 “Interface drug database”. The work that is being performed within the Task 8.2, as well as within the whole WP8, is a continuous process, and will be concluded in D8.4 “Development report tool”.

Different drugs such as Disopyramide, Digoxin, Mavacamten, 2-deoxy adenosine triphosphate (dATP) with fitted parameters from MUSICO which reacted through three characteristic pathways of drug flow have been described. Disopyramide and Mavacamten are described with their effects on the macroscopic parameters inside the SILICOFCM platform.

The corresponding PV diagrams in the PAK finite element solver for different Ca+ concentration, displacement (deformation), velocity and pressure field with analysis of ejection fraction and wall elasticity has been presented. The activation sequences which correspond to ECG signals were compared with real ECG measurement at V1 from clinical partners.

A number of different scenarios of using SILICOFCM platform for various drugs testing for basic cardiac function have been presented. Initial comparison of the *in silico* with main clinical parameters as PV diagram, systemic pressure, input and output blood flow velocity from left ventricle, ejection fraction, ECG measurements on body surface on the real patients are very promising for SILICOFCM platform as software as medical device as well as for research purposes.

6. References

The references are inserted as footnotes.